
Contrastive Learning for Unsupervised Domain Adaptation of Time Series

Yilmazcan Ozyurt
 ETH Zürich
 yozyurt@ethz.ch

Stefan Feuerriegel
 LMU Munich
 feuerriegel@lmu.de

Ce Zhang
 ETH Zürich
 ce.zhang@inf.ethz.ch

Abstract

Unsupervised domain adaptation (UDA) aims at learning a machine learning model using a labeled source domain that performs well on a similar yet different, unlabeled target domain. UDA is important in many applications such as medicine, where it is used to adapt risk scores across different patient cohorts. In this paper, we develop a novel framework for UDA of time series data, called CLUDA. Specifically, we propose a contrastive learning framework to learn contextual representations in multivariate time series, so that these preserve label information for the prediction task. In our framework, we further capture the variation in the contextual representations between source and target domain via a custom nearest-neighbor contrastive learning. To the best of our knowledge, ours is the first framework to learn domain-invariant, contextual representation for UDA of time series data. We evaluate our framework using a wide range of time series datasets to demonstrate its effectiveness and show that it achieves state-of-the-art performance for time series UDA.

1 Introduction

Many real-world applications of machine learning are characterized by differences between the domains at training and deployment [22, 27]. Therefore, effective methods are needed that learn domain-invariant representations across domains. For example, it is well known that medical settings suffer from substantial domain shifts due to differences in patient cohorts, medical routines, reporting practices, etc. [15, 57]. Hence, a machine learning model trained for one patient cohort may not generalize to other patient cohorts. This highlights the need for effective domain adaptation of time series.

Unsupervised domain adaptation (UDA) aims to learn a machine learning model using a labeled source domain that performs well on a similar yet different, unlabeled target domain [16, 30]. So far, many methods for UDA have been proposed for *computer vision* [7, 16, 23, 25, 30, 35, 40, 41, 43, 44, 49, 50, 53, 59].

In contrast, comparatively few works have focused on UDA of *time series*. Here, previous works utilize a tailored feature extractor to capture temporal dynamics of multivariate time series, typically through recurrent neural networks (RNNs) [36], long short-term memory (LSTM) networks [5], and convolutional neural networks [29, 51, 52]. Some of these works minimize the domain discrepancy of learned features via adversarial-based methods [36, 51, 52] or restrictions through metric-based methods [5, 29].

Another research stream has developed time series methods for *transfer learning* from the source domain to the target domain [13, 14, 26, 48, 54–56]. These methods pre-train a neural network model via contrastive learning to capture the contextual representation of time series from unlabeled source domain. However, these methods operate on a labeled target domain, which is different from UDA.

To the best of our knowledge, there is no method for UDA of time series that captures and aligns the contextual representation across source and target domains.

In this paper, we propose a novel framework for unsupervised domain adaptation of time series data based on contrastive learning, called CLUDA. Different from existing works, our CLUDA framework aims at capturing the contextual representation in multivariate time series as a form of high-level features. To accomplish this, we incorporate the following components: (1) We minimize the domain discrepancy between source and target domains through adversarial training. (2) We capture the contextual representation by generating positive pairs via a set of semantic-preserving augmentations and then learning their embeddings. For this, we make use of contrastive learning (CL). (3) We further align the contextual representation across source and target domains via a custom nearest-neighborhood contrastive learning.

We evaluate our method using a wide range of time series datasets. (1) We conduct extensive experiments using established **benchmark datasets** WISDM [28], HAR [1], and HHAR [42]. Thereby, we show our CLUDA leads to increasing accuracy on target domains by an important margin. (2) We further conduct experiments on two large-scale, *real-world medical datasets*, namely MIMIC-IV [24] and AmsterdamUMCdb [45]. We demonstrate the effectiveness of our framework for our medical setting and confirm its superior performance over state-of-the-art baselines. In fact, medical settings are known to suffer from substantial domain shifts (e.g., due to different patient cohorts, medical routines, reporting practices, etc., across health institutions) [15, 32, 57]. This highlights the relevance and practical need for adapting machine learning across domains from training and deployment.

Contributions:¹

1. We propose a novel, contrastive learning framework (CLUDA) for unsupervised domain adaptation of time series. To the best of our knowledge, ours is the first that learns a contextual representation of multivariate time series to preserve information on labels.
2. We capture domain-invariant, contextual representations in CLUDA through a custom approach combining nearest-neighborhood contrastive learning and adversarial learning to align them across domains.
3. We demonstrate that our CLUDA achieves state-of-the-art performance. Furthermore, we show the practical value of our framework using large-scale, real-world medical data from intensive care units.

2 Related Work

Contrastive learning: Contrastive learning aims to learn representations with self-supervision, so that similar samples are embedded close to each other (positive pair) while pushing dissimilar samples (negative pairs). Such representations have been shown to capture the semantic information of the samples by maximizing the lower bound of the mutual information between two augmented views [2, 46, 47]. Several methods for contrastive learning have been developed so far [33, 8, 12, 21], and several of which are tailored to unsupervised representation learning of time series [14, 55, 56, 48, 26, 13, 54, 58]. A detailed review is in Appendix A.

Unsupervised domain adaptation: Unsupervised domain adaptation leverages labeled source domain to predict the labels of a different, unlabeled target domain [16]. To achieve this, UDA methods typically aim to minimize the domain discrepancy and thereby decrease the lower bound of the target error [4]. To minimize the domain discrepancy, existing UDA methods can be loosely grouped into three categories: (1) *Adversarial-based methods* reduce the domain discrepancy via domain discriminator networks, which enforce the feature extractor to learn domain-invariant feature representations. Examples are domain adversarial neural network (DANN) [16], conditional domain adversarial network (CDAN) [30], adversarial discriminative domain adaptation (ADDA) [50], multi-adversarial domain adaptation (MADA) [35], decision-boundary iterative refinement training with a teacher (DIRT-T) [40], and adversarial domain adaptation with domain mixup (DM-ADA) [53]. (2) *Contrastive methods* reduce the domain discrepancy through a minimization of a contrastive loss which aims to bring source and target embeddings of the same class together. Here, the labels (i.e., class

¹Codes are available at <https://github.com/oezyurty/CLUDA>.

information) of the target samples are unknown, and, hence, these methods rely on pseudo-labels of the target samples generated from a clustering algorithm, which are noisy estimates of the actual labels of the target samples. Examples are contrastive adaptation network (CAN) [25], contrastive learning framework for semi-supervised domain adaptation (CLDA) [41], gradient regularized contrastive learning (GRCL) [44], and historical contrastive learning (HCL) [23]. (3) *Metric-based methods* reduce the domain discrepancy by enforcing restrictions through a certain distance metric (e.g., via regularization). Examples are deep domain confusion (DDC) [49], correlation alignment via deep neural networks (Deep CORAL) [43], deep subdomain adaptation network (DSAN) [59], higher-order moment matching (HoMM) [7], and minimum discrepancy estimation for deep domain adaptation (MMDA) [38]. However, previous works on UDA typically come from computer vision and, therefore, are not directly applicable to time series. In contrast, comparatively few works have been proposed for UDA of time series (see below).

Unsupervised domain adaptation for time series: A few methods have been tailored to unsupervised domain adaptation for time series data. Variational recurrent adversarial deep domain adaptation (VRADA) [36] was the first UDA method for multivariate time series that uses adversarial learning for reducing domain discrepancy. In VRADA, the feature extractor is a variational recurrent neural network [11], and VRADA then trains the classifier and the domain discriminator (adversarially) for the last latent variable of its variational recurrent neural network. Convolutional deep domain adaptation for time series (CoDATS) [51] builds upon the same adversarial training as VRADA, but uses convolutional neural network for the feature extractor instead. Time series sparse associative structure alignment (TS-SASA) [5] is a metric-based method. Here, intra-variables and inter-variables attention mechanisms are aligned between the domains via the minimization of maximum mean discrepancy (MMD). Adversarial spectral kernel matching (AdvSKM) [29] is another metric-based method that aligns the two domains via MMD. Specifically, it introduces a spectral kernel mapping, from which the output is used to minimize MMD between the domains. Across all of the aforementioned methods, the aim is to align the features across source and target domains. There are some extensions for specialized problems. For instance, CALDA [52] is a neural network similar to CoDATS but is tailored for multi-source domains, and it is thus not applicable our setting later.

Research gap: For UDA of time series, existing works merely align the *features* across source and target domains. In contrast to that, we propose to align the *contextual representation*. To achieve this, we develop a novel framework called CLUDA based on contrastive learning.

3 Problem Definition

We consider a classification task for which we aim to perform *unsupervised domain adaptation of time series*. Specifically, we have two distributions over the time series from the source domain \mathcal{D}_S and the target domain \mathcal{D}_t . In our setup, we have **labeled** *i.i.d.* samples from the source domain given by $\mathcal{S} = \{(x_i^s, y_i^s)\}_{i=1}^{N_s} \sim \mathcal{D}_S$, where x_i^s is a sample of the source domain, y_i^s is the label for the given sample, and N_s is the overall number of *i.i.d.* samples from the source domain. In contrast, we have **unlabeled** *i.i.d.* samples from the target domain given by $\mathcal{T} = \{x_i^t\}_{i=1}^{N_t} \sim \mathcal{D}_T$, where x_i^t is a sample of the target domain and N_t is the overall number of *i.i.d.* samples from the target domain. For brevity, we omit the index i (i.e., x^s instead of x_i^s) when it is clear from the context.

In this paper, we allow for multivariate time series. Hence, each x_i (either from the source or target domain) is a sample of multivariate time series denoted by $x_i = \{x_{it}\}_{t=1}^T \in \mathbb{R}^{M \times T}$, where T is the number of time steps and $x_{it} \in \mathbb{R}^M$ is M observations for the corresponding time step.

Our aim is to build a classifier that generalizes well over target samples \mathcal{T} by leveraging the labeled source samples \mathcal{S} . Importantly, labels for the target domain are **not** available during training. Instead, we later use the labeled target samples $\mathcal{T}_{\text{test}} = \{(x_i^t, y_i^t)\}_{i=1}^{N_{\text{test}}} \sim \mathcal{D}_T$ only for the purpose of evaluating our framework.

The above setting is directly relevant for practice [15, 22, 27, 57]. For example, medical time series from different health institutions differ in terms of patient cohorts, medical routines, reporting practice, etc., and, therefore, are subject to substantial domain shifts. As such, data from training and data from deployment should be considered as different domains. Hence, in order to apply machine learning for risk scoring or other medical use cases, it is often helpful to adapt the machine learning model trained on one domain \mathcal{S} for another domain \mathcal{T} before deployment.

4 Proposed CLUDA Framework

In this section, we describe the components of our framework to learn domain-invariant, contextual representation of time series. We start with an overview of the neural architecture, and then describe how we (1) perform adversarial training, (2) capture the contextual representation, and (3) align contextual representation across domains.

4.1 Architecture

The neural architecture of our CLUDA for unsupervised domain adaptation of time series is shown in Fig. 1. Specifically, the components are as follows: (1) The **feature extractor** network $F(\cdot)$ takes the original time series x^s and x^t from both domains and creates corresponding embeddings z^s and z^t , respectively. (2) The **classifier network** $C(\cdot)$ is trained to predict the label y^s of time series from the source domain using the embeddings z^s . (3) The **discriminator network** $D(\cdot)$ is trained to distinguish source embeddings z^s from target embeddings z^t . For such training, we introduce domain labels $d = 0$ for source instances and $d = 1$ for target instances.

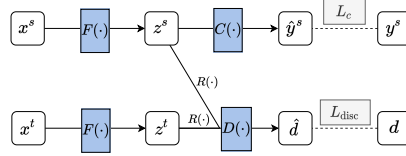


Figure 1: High-level overview of the neural architecture with adversarial domain adaptation.

4.2 Adversarial Training for Unsupervised Domain Adaptation

To train the above components, we minimize a combination of two losses: (1) Our *prediction loss* L_c trains the feature extractor $F(\cdot)$ and the classifier $C(\cdot)$. We train both jointly in order to correctly predict the labels from the source domain. For this, we define the prediction loss

$$L_c = \frac{1}{N_s} \sum_i^{N_s} L_{\text{pred}}(C(F(x_i^s)), y_i^s), \quad (1)$$

where $L_{\text{pred}}(\cdot, \cdot)$ is the cross-entropy loss.

(2) Our *domain classification loss* L_{disc} is used to learn domain-invariant feature representations. Here, we use adversarial learning [16]. To this end, the domain discriminator $D(\cdot)$ is trained to minimize the domain classification loss, whereas the feature extractor $F(\cdot)$ is trained to maximize the same loss simultaneously. This is achieved by the gradient reversal layer $R(\cdot)$ between $F(\cdot)$ and $D(\cdot)$, defined by

$$R(x) = x, \quad \frac{dR}{dx} = -\mathbf{I}. \quad (2)$$

Hence, we yield the domain classification loss

$$L_{\text{disc}} = \frac{1}{N_s} \sum_i^{N_s} L_{\text{pred}}(D(R(F(x_i^s))), d_i^s) + \frac{1}{N_t} \sum_i^{N_t} L_{\text{pred}}(D(R(F(x_i^t))), d_i^t). \quad (3)$$

4.3 Capturing Contextual Representations

In our CLUDA, we capture a contextual representation of the time series in the embeddings z^s and z^t , and then align the contextual representations of the two domains for unsupervised domain adaptation. With this approach, we improve upon the earlier works in two ways: (1) We encourage our feature extractor $F(\cdot)$ to learn label-preserving information captured by the context. This observation was made earlier for unsupervised representation learning yet outside of our time series settings [2, 8, 9, 17, 19, 46, 47]. (2) We further hypothesize that discrepancy between the contextual representations of two domains is smaller than the discrepancy between their feature space, and therefore, the domain alignment task becomes easier.

To capture the contextual representations of time series for each domain, we leverage contrastive learning. CL is widely used in unsupervised representation learning for the downstream tasks in machine learning [8, 9, 21, 31, 39, 55, 58]. In plain words, CL approach aims to learn similar representations for two augmented views (positive pair) of the same sample in contrast to the views from other samples (negative pairs). This leads to a maximization of the mutual information between two views and, therefore, captures a contextual representation [2, 46, 47].

In our framework (see Fig. 2), we leverage contrastive learning in form of momentum contrast (MoCo) [21] in order to capture the contextual representations from each domain. Accordingly, we apply semantic-preserving augmentations [10, 26, 55] to each sample of multivariate time series twice. Specifically, in our framework, we sequentially apply the following functions with random instantiations: history crop, history cutout, channel dropout, and Gaussian noise (see Appendix C for details). After augmentation, we have two views of each sample, called query x_q and key x_k . These two views are then processed by the feature extractor to get their embeddings as $z_q = F(x_q)$ and $z_k = \tilde{F}(x_k)$. Here, $\tilde{F}(\cdot)$ is a *momentum-updated* feature extractor for MoCo.

To train the momentum-updated feature extractor, the gradients are not backpropagated through $\tilde{F}(\cdot)$. Instead, the weights $\theta_{\tilde{F}}$ are updated by the momentum via

$$\theta_{\tilde{F}} \leftarrow m \theta_{\tilde{F}} + (1 - m) \theta_F, \quad (4)$$

where $m \in [0, 1]$ is the momentum coefficient. The objective of MoCo-based contrastive learning is to project z_q via a projector network $Q(\cdot)$ and bring the projection $Q(z_q)$ closer to its positive sample z_k (as opposed to negative samples stored in queue $\{z_{kj}\}_{j=1}^J$). After each training step, the batch of z_k 's are stored in queue of size J . As a result, for each domain, we have the following *contrastive loss*

$$L_{\text{CL}} = -\frac{1}{N} \sum_{i=1}^N \log \frac{\exp(Q(z_{qi}) \cdot z_{ki}/\tau)}{\exp(Q(z_{qi}) \cdot z_{ki}/\tau) + \sum_{j=1}^J \exp(Q(z_{qi}) \cdot z_{kj}/\tau)}, \quad (5)$$

where $\tau > 0$ is the temperature scaling parameter, and where all embeddings are normalized. Since we have two domains (i.e., source and target), we also have two contrastive loss components given by L_{CL}^s and L_{CL}^t and two queues given by queue^s and queue^t , respectively.

Fig. 2 shows some network components for source and target samples twice for better readability, even though the weights of $F(\cdot)$, $\tilde{F}(\cdot)$, and $Q(\cdot)$ are actually shared across domains. We further plot the discriminator $D(\cdot)$ separately to avoid overlapping arrows in the figure.

4.4 Aligning the Contextual Representation Across Domains

Our CLUDA framework further aligns the contextual representation across the source and target domains. To do so, we build upon ideas for nearest-neighbor contrastive learning [12] from unsupervised representation learning, yet outside of our time series setting. To the best of our knowledge, ours is the first nearest-neighbor contrastive learning approach for unsupervised domain adaptation of time series.

In our CLUDA framework, nearest-neighbor contrastive learning should facilitate the classifier $C(\cdot)$ to make accurate predictions for the target domain. We achieve this by creating positive pairs between domains, whereby we explicitly align the representations across domains. For this, we pair z_{qi}^t with the nearest-neighbor of z_{ki}^s from the source domain, denoted as $NN_s(z_{ki}^s)$. We thus introduce our *nearest-neighbor contrastive learning loss*

$$L_{\text{NNCL}} = -\frac{1}{N_t} \sum_{i=1}^{N_t} \log \frac{\exp(z_{qi}^t \cdot NN_s(z_{ki}^s)/\tau)}{\sum_{j=1}^{N_s} \exp(z_{qi}^t \cdot z_{qj}^s/\tau)}, \quad (6)$$

where $NN_s(\cdot)$ retrieves the nearest-neighbor of an embedding from the source queries $\{z_{qi}^s\}_{i=1}^{N_s}$.

4.5 Training

Overall loss: Overall, our CLUDA framework minimizes

$$L = L_c + \lambda_{\text{disc}} \cdot L_{\text{disc}} + \lambda_{\text{CL}} \cdot (L_{\text{CL}}^s + L_{\text{CL}}^t) + \lambda_{\text{NNCL}} \cdot L_{\text{NNCL}}, \quad (7)$$

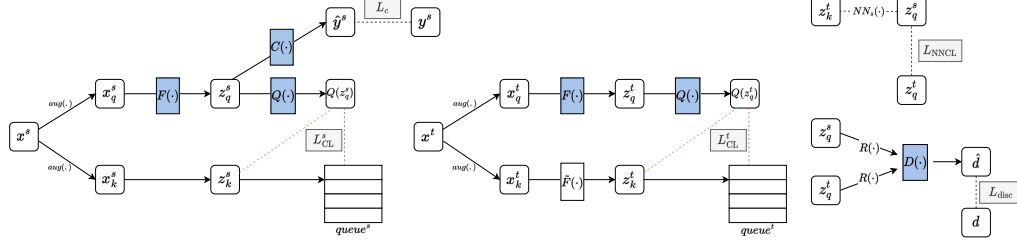


Figure 2: The complete CLUDA framework.

where hyperparameters λ_{disc} , λ_{CL} , and λ_{NNCL} control the contribution of each component.

Implementation: We implement the feature extractor $F(\cdot)$ via a temporal convolutional network (TCN) [3]. We configure its kernel size, dilation factor and number of layers to cover the entire history of the time series for each dataset. We implement the discriminator $D(\cdot)$, the classifier $C(\cdot)$, and the projector $Q(\cdot)$ via multilayer perceptrons with one hidden-layer. Appendix C provides all details of our architecture search for each component.

5 Experimental Setup

Our evaluation is two-fold: (1) We conduct extensive experiments using established **benchmark datasets**, which have been used in the earlier works of UDA on time series [51, 52, 5, 29]. Thereby, we show how our CLUDA leads to increasing accuracy on target domains by an important margin. (2) We show the applicability of our framework in a *real-world* setting with **medical datasets**.

(1) Benchmark datasets: We follow previous literature for a fair comparison. For this, we include three sensor datasets in our experiments: (i) The WISDM dataset [28] contains the accelerometer data of 30 participants. (ii) The Human activity recognition (HAR) dataset [1] collects accelerometer, gyroscope, and estimated body acceleration data from 30 participants. (iii) The Heterogeneity Human Activity Recognition (HHAR) dataset [42] contains the accelerometer data from 9 participants. For each dataset, we consider each participant as a separate domain, and we randomly sample 10 source-target domain pairs for evaluation. Further details are in Appendix B.

(2) Medical datasets: We use MIMIC-IV [24] and AmsterdamUMCdb [45]. Both are de-identified, publicly-available data from intensive care unit stays, where the goal is to predict mortality. To date, MIMIC-IV is the largest public dataset for intensive care units with 49,351 ICU stays; AmsterdamUMCdb contains 19,840 ICU stays. However, both have a different origin (Boston, United States vs. Amsterdam, Netherlands) and thus reflect patients with different characteristics, medical procedures, etc. For the medical datasets, we follow the literature [36, 5] and create 4 domains based on patients' age groups: 20–45, 46–65, 66–85, and 85+ years. We then apply UDA for each cross-domain scenario (i.e., from Group 1 \mapsto Group 4 to Group 4 \mapsto Group 3) to predict mortality.

Baselines: (1) We report the performance of a model without UDA (**w/o UDA**) to show the overall contribution of UDA methods. For this, we only use feature extractor $F(\cdot)$ and the classifier $C(\cdot)$ using the same architecture as in our CLUDA. This model is only trained on the source domain. (2) We implement the following state-of-the-art baselines for UDA of time series data. These are: **VRADA** [36], **CoDATS** [51], **TS-SASA** [5], and **AdvSKM** [29]. In our results later, we omitted TS-SASA as it repeatedly was not better than random. (3) We additionally implement **CAN** [25], **CDAN** [30], **DDC** [49], **DeepCORAL** [43], **DSAN** [59], **HoMM** [7], and **MMDA** [38]. These models were originally developed for computer vision, but we tailored their feature extractor to time series (i.e., by setting it to a temporal convolutional network). See Appendix C for all details.

6 Results

6.1 Prediction Performance on Benchmark Datasets

Figure 3a shows the average accuracy of each method for 10 source-target domain pairs on the WISDM, HAR, and HHAR datasets. On WISDM dataset, our CLUDA outperforms the best baseline

accuracy of CoDATS by 12.7 % (0.754 vs. 0.669). On HAR dataset, our CLUDA outperforms the best baseline accuracy of CDAN by 18.9 % (0.944 vs. 0.794). On HHAR dataset, our CLUDA outperforms the best baseline accuracy of CDAN by 21.8 % (0.759 vs. 0.623). Overall, CLUDA consistently improves the best UDA baseline performance by a large margin. In Appendix D, we provide the full list of UDA results for each source-target pair, and additionally provide Macro-F1 scores, which confirm our findings from above.

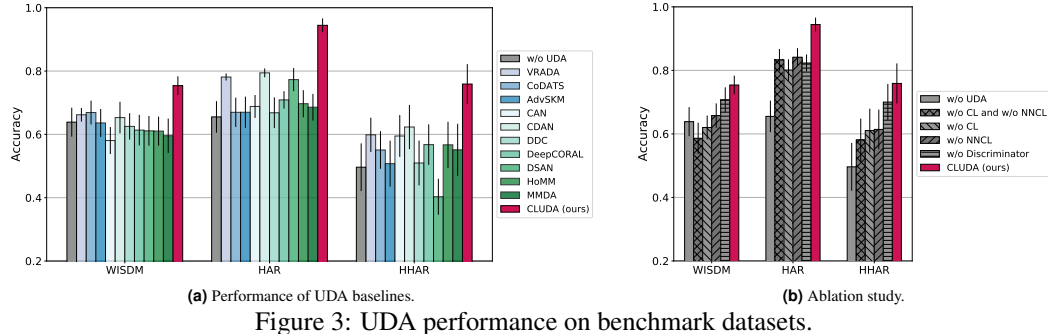


Figure 3: UDA performance on benchmark datasets.

Insights: We further visualize the embeddings in Fig. 4 to study the domain discrepancy and how our CLUDA aligns the representation of time series. (a) The embeddings of w/o UDA show that there is a significant domain shift between source and target. This can be observed by the two clusters of each class (i.e., one for each domain). (b) CDAN as the best baseline reduces the domain shift by aligning the features of source and target for some classes, yet it mixes the different classes of the different domains (e.g., blue class of source and green class of target overlap). (c) By examining the embeddings from our CLUDA, we confirm its effectiveness: (1) Our CLUDA pulls together the source (target) classes for the source (target) domain (due to the CL). (2) Our CLUDA further pulls both source and target domains together for each class (due to the alignment). Plots for all other methods are in Appendix E.

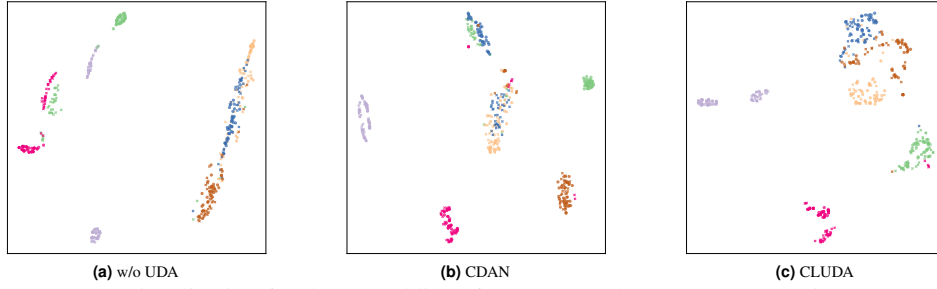


Figure 4: t-SNE visualization for the embeddings from HHAR dataset. Each class is represented by a different color. Shape shows source and target domains (circle vs. cross).

Ablation study: We conduct an ablation study (see Fig. 3b) to better understand the importance of the different components in our framework. The variants are: (1) **w/o UDA** baseline for comparison; (2) **w/o CL and w/o NNCL**, which refers to base architecture from Sec. 4.2; (3) **w/o CL**, which deactivates CL (from Sec. 4.3) for capturing contextual representations; (4) **w/o NNCL**, which deactivates NNCL (from Sec. 4.4) for aligning contextual representations across domains; and (5) **w/o Discriminator**, which deactivates the discriminator. Overall, the low accuracy of **w/o CL and w/o NNCL** demonstrates the importance of capturing and aligning the contextual representations. Comparing **w/o Discriminator** shows that the largest part of our performance improvements (compared to **w/o UDA**) comes from our novel components introduced in Sec. 4.3 and Sec. 4.4 to capture and align the contextual representation of time series. The discriminator also helps achieving consistent performance gains, albeit of smaller magnitude. Finally, our CLUDA works the best in all experiments, thereby justifying our chosen architecture. See Appendix F for the detailed results of our ablation study.

6.2 Prediction Performance on Medical Datasets

We further demonstrate that our CLUDA achieves state-of-the-art UDA performance using the medical datasets. For this, Table 1 lists 12 UDA scenarios created from the MIMIC dataset. In 9 out of 12 domain UDA scenarios, CLUDA yields the best mortality prediction in the target domain, consistently outperforming the UDA baselines. When averaging over all scenarios, our CLUDA improves over the performance of the best baseline (AdvSKM) by 2.2 % (AUROC 0.773 vs. 0.756). Appendix H reports the ablation study for this experimental setup with similar findings as above.

Appendix G repeats the experiments for another medical dataset: AmsterdamUMCdb [45]. Again, our CLUDA achieves state-of-the-art performance.

Table 1: Prediction performance for medical dataset. Task: mortality prediction between various age groups of MIMIC-IV. Shown: mean AUROC over 10 random initializations.

Sour \mapsto Tar	w/o UDA	VRADA	CoDATS	AdvSKM	CAN	CDAN	DDC	DeepCORAL	DSAN	HoMM	MMDA	CLUDA (ours)
1 \mapsto 2	0.744	0.786	0.744	0.757	0.757	0.726	0.745	0.728	0.756	0.742	0.726	0.798
1 \mapsto 3	0.685	0.729	0.685	0.702	0.687	0.654	0.694	0.688	0.701	0.654	0.684	0.747
1 \mapsto 4	0.617	0.631	0.616	0.619	0.607	0.580	0.613	0.595	0.620	0.587	0.622	0.649
2 \mapsto 1	0.818	0.828	0.822	0.835	0.804	0.842	0.821	0.824	0.821	0.820	0.825	0.856
2 \mapsto 3	0.790	0.746	0.797	0.792	0.789	0.788	0.791	0.789	0.795	0.797	0.793	<u>0.796</u>
2 \mapsto 4	0.696	0.649	0.699	0.696	0.666	0.620	0.693	0.699	0.690	0.694	0.694	<u>0.697</u>
3 \mapsto 1	0.787	0.808	0.788	0.798	0.800	0.754	0.796	0.797	0.790	0.796	0.803	0.822
3 \mapsto 2	0.833	0.805	0.832	0.835	0.837	0.777	0.831	0.827	0.833	0.834	0.830	0.843
3 \mapsto 4	0.751	0.684	0.748	0.745	0.727	0.689	0.748	0.746	<u>0.750</u>	0.733	0.745	0.745
4 \mapsto 1	0.783	0.790	0.783	0.788	0.792	0.747	0.778	0.768	0.766	0.774	0.754	0.807
4 \mapsto 2	0.761	0.760	0.762	0.765	0.765	0.748	0.761	0.740	0.757	0.756	0.744	0.769
4 \mapsto 3	0.736	0.723	0.737	0.734	0.731	0.730	0.739	0.734	0.735	0.742	0.738	0.748
Avg	0.750	0.745	0.751	0.756	0.747	0.721	0.751	0.745	0.751	0.744	0.747	0.773

Higher is better. Best value in bold. Second best results are underlined if std. dev. overlap.

6.3 Case Study: Application to Medical Practice

We now provide a case study showing the application of our framework to medical practice. Here, we evaluate the domain adaptation between two health institutions. We intentionally chose this setting as medical applications are known to suffer from a substantial domain shifts (e.g., due to different patient cohorts, medical routines, reporting practices, etc., across health institutions) [15, 32, 57]. We treat MIMIC and AmsterdamUMCdb (AUMC) as separate domains and then predict health outcomes analogous to earlier works [5, 6, 18, 34, 36]: decompensation, mortality, and length of stay (see Table 2). All details regarding the medical datasets (i.e., summary statistics, measurements, pre-processing etc.) and task definitions are given in Appendix B.

Fig. 5 shows the performance across all three UDA tasks and for both ways (i.e., MIMIC \mapsto AUMC and AUMC \mapsto MIMIC). For better comparability in practice, we focus on the “*performance gap*”: we interpret the performance from source \mapsto source setting as a loose upper bound.² We then report how much of the performance gap between no domain adaptation (w/o UDA) vs. the loose upper bound is filled by each method. Importantly, our CLUDA consistently outperforms the state-of-the-art baselines. For instance, in decompensation prediction for AUMC, our CLUDA (AUROC 0.791) fills 47.6 % of the performance gap between no domain adaptation (AUROC 0.771) and loose upper bound from the source \mapsto source setting

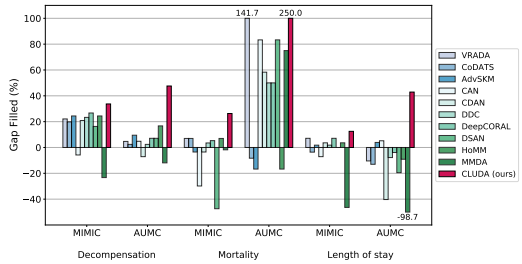


Figure 5: Case study. Report is how much of the performance gap [%] is filled by each method. Here: performance gap [%] is the difference between no domain adaptation and the source \mapsto source setting as a loose upper bound on performance.

²In some cases, this loose upper bound can be exceeded by UDA methods. For instance, when there is not enough number of samples in target domain. Then, leveraging a larger and labeled dataset as source domain can yield a superior performance.

Table 2: 3 UDA tasks between MIMIC and AUMC. Shown: Average performance over 10 random initializations.

Task	Decompensation (AUROC)				Mortality (AUROC)				Length-of-stay (KAPPA)			
	Source		MIMIC	AUMC	Target		MIMIC	AUMC	AUMC	MIMIC	MIMIC	AUMC
Source	MIMIC	AUMC	AUMC	MIMIC	MIMIC	AUMC	MIMIC	MIMIC	MIMIC	MIMIC	AUMC	AUMC
w/o UDA	0.831	0.771	0.813	0.745	0.831	0.709	0.721	0.774	0.178	0.169	0.246	0.122
VRADA	0.817	0.773	0.798	0.764	0.827	0.726	0.729	0.778	0.168	0.161	0.241	0.126
CoDATS	0.825	0.772	0.818	0.762	0.832	0.708	0.724	0.778	0.174	0.159	0.243	0.120
AdvSKM	0.824	0.775	0.817	0.766	0.830	0.707	0.724	0.772	0.179	0.172	0.244	0.123
CAN	0.825	0.773	0.807	0.740	0.830	0.719	0.715	0.757	0.142	0.173	0.233	0.118
CDAN	0.824	0.768	0.817	0.763	0.776	0.716	0.712	0.772	0.176	0.138	0.244	0.124
DDC	0.825	0.772	0.819	0.765	0.831	0.715	0.721	0.776	0.175	0.163	0.244	0.123
DeepCORAL	0.832	0.774	0.819	0.768	0.832	0.715	0.727	0.777	0.175	0.166	0.244	0.126
DSAN	0.831	0.774	0.808	0.759	0.832	0.719	0.721	0.747	0.175	0.154	0.246	0.122
HoMM	0.829	0.778	0.816	0.766	0.833	0.707	0.720	0.778	0.174	0.162	0.243	0.124
MMDA	0.821	0.766	0.814	0.725	0.831	0.718	0.724	0.773	0.158	0.093	0.246	0.096
CLUDA (ours)	0.832	0.791	0.825	0.774	0.836	0.739	0.750	0.789	0.216	0.202	0.276	0.129

Higher is better. Best value in bold. Black font: main results for UDA. Gray font: source \leftrightarrow source.

(AUROC 0.813). In contrast, the best baseline model of this task (HoMM) can only fill 16.7% (AUROC 0.778). Altogether, this demonstrates the effectiveness of our proposed framework.

Appendix I reports the detailed results for different performance metrics. Appendix J provides an ablation study. Both support our above findings.

7 Conclusion

In this paper, we propose a novel framework for unsupervised domain adaptation (UDA) of time series based on contrastive learning, called CLUDA. To the best of our knowledge, CLUDA is the first approach that learns domain-invariant, contextual representation in multivariate time series for UDA. Further, CLUDA achieves state-of-the-art performance for UDA of time series. Importantly, our two novel components – i.e., our custom CL and our NNCL – yield clear performance improvements. Finally we expect our framework of direct practical value for medical applications where risk scores should be transferred across populations or institutions.

Acknowledgments and Disclosure of Funding

We thank Alexander von Ehr for domain expertise and academic guidance. The author list was determined with respect to institutional guidelines.

References

- [1] Davide Anguita, Alessandro Ghio, Luca Oneto, Xavier Parra Perez, and Jorge Luis Reyes Ortiz. A public domain dataset for human activity recognition using smartphones. In *ESANN*, 2013.
- [2] Philip Bachman, R Devon Hjelm, and William Buchwalter. Learning representations by maximizing mutual information across views. *NeurIPS*, 2019.
- [3] Shaojie Bai, J Zico Kolter, and Vladlen Koltun. An empirical evaluation of generic convolutional and recurrent networks for sequence modeling. *arXiv preprint arXiv:1803.01271*, 2018.
- [4] Shai Ben-David, John Blitzer, Koby Crammer, Alex Kulesza, Fernando Pereira, and Jennifer Wortman Vaughan. A theory of learning from different domains. *JMLR*, 79:151–175, 2010.
- [5] Ruichu Cai, Jiawei Chen, Zijian Li, Wei Chen, Keli Zhang, Junjian Ye, Zhuozhang Li, Xiaoyan Yang, and Zhenjie Zhang. Time series domain adaptation via sparse associative structure alignment. In *AAAI*, 2021.
- [6] Zhengping Che, Sanjay Purushotham, Kyunghyun Cho, David Sontag, and Yan Liu. Recurrent neural networks for multivariate time series with missing values. *Scientific Reports*, 2018.
- [7] Chao Chen, Zhihang Fu, Zhihong Chen, Sheng Jin, Zhaowei Cheng, Xinyu Jin, and Xian-Sheng Hua. Homm: Higher-order moment matching for unsupervised domain adaptation. In *AAAI*, 2020.
- [8] Ting Chen, Simon Kornblith, Mohammad Norouzi, and Geoffrey Hinton. A simple framework for contrastive learning of visual representations. In *ICML*, 2020.
- [9] Xinlei Chen, Haoqi Fan, Ross Girshick, and Kaiming He. Improved baselines with momentum contrastive learning. *arXiv preprint arXiv:2003.04297*, 2020.
- [10] Joseph Y Cheng, Hanlin Goh, Kaan Dogrusoz, Oncel Tuzel, and Erdrin Azemi. Subject-aware contrastive learning for biosignals. *arXiv preprint arXiv:2007.04871*, 2020.
- [11] Junyoung Chung, Kyle Kastner, Laurent Dinh, Kratarth Goel, Aaron C Courville, and Yoshua Bengio. A recurrent latent variable model for sequential data. *NeurIPS*, 2015.
- [12] Debidatta Dwibedi, Yusuf Aytar, Jonathan Tompson, Pierre Sermanet, and Andrew Zisserman. With a little help from my friends: Nearest-neighbor contrastive learning of visual representations. In *ICCV*, 2021.
- [13] Emadeldeen Eldele, Mohamed Ragab, Zhenghua Chen, Min Wu, Chee Keong Kwok, Xiaoli Li, and Cuntai Guan. Time-series representation learning via temporal and contextual contrasting. In *IJCAI*, 2021.
- [14] Jean-Yves Franceschi, Aymeric Dieuleveut, and Martin Jaggi. Unsupervised scalable representation learning for multivariate time series. *NeurIPS*, 2019.
- [15] Joseph Futoma, Morgan Simons, Trishan Panch, Finale Doshi-Velez, and Leo Anthony Celi. The myth of generalisability in clinical research and machine learning in health care. *The Lancet Digital Health*, 2(9), 2020.
- [16] Yaroslav Ganin, Evgeniya Ustinova, Hana Ajakan, Pascal Germain, Hugo Larochelle, François Laviolette, Mario Marchand, and Victor Lempitsky. Domain-adversarial training of neural networks. *JMLR*, 17: 2096–2030, 2016.
- [17] Songwei Ge, Shlok Mishra, Chun-Liang Li, Haohan Wang, and David Jacobs. Robust contrastive learning using negative samples with diminished semantics. *NeurIPS*, 2021.
- [18] Wendong Ge, Jin-Won Huh, Yu Rang Park, Jae-Ho Lee, Young-Hak Kim, and Alexander Turchin. An interpretable icu mortality prediction model based on logistic regression and recurrent neural networks with lstm units. In *AMIA Annual Symposium Proceedings*, 2018.
- [19] Jean-Bastien Grill, Florian Strub, Florent Altché, Corentin Tallec, Pierre Richemond, Elena Buchatskaya, Carl Doersch, Bernardo Avila Pires, Zhaohan Guo, Mohammad Gheshlaghi Azar, et al. Bootstrap your own latent – a new approach to self-supervised learning. *NeurIPS*, 2020.
- [20] Hrayr Harutyunyan, Hrant Khachatrian, David C Kale, Greg Ver Steeg, and Aram Galstyan. Multitask learning and benchmarking with clinical time series data. *Scientific Data*, 2019.
- [21] Kaiming He, Haoqi Fan, Yuxin Wu, Saining Xie, and Ross Girshick. Momentum contrast for unsupervised visual representation learning. In *CVPR*, 2020.

[22] Dan Hendrycks and Thomas Dietterich. Benchmarking neural network robustness to common corruptions and perturbations. In *ICLR*, 2019.

[23] Jiaxing Huang, Dayan Guan, Aoran Xiao, and Shijian Lu. Model adaptation: Historical contrastive learning for unsupervised domain adaptation without source data. *NeurIPS*, 2021.

[24] Alistair Johnson, Lucas Bulgarelli, Tom Pollard, Steven Horng, Leo Anthony Celi, and R Mark IV. MIMIC-IV. *PhysioNet*, 2020.

[25] Guoliang Kang, Lu Jiang, Yi Yang, and Alexander G Hauptmann. Contrastive adaptation network for unsupervised domain adaptation. In *CVPR*, 2019.

[26] Dani Kiyasseh, Tingting Zhu, and David A Clifton. Clocs: Contrastive learning of cardiac signals across space, time, and patients. In *ICML*, 2021.

[27] Pang Wei Koh, Shiori Sagawa, Henrik Marklund, Sang Michael Xie, Marvin Zhang, Akshay Balsubramani, Weihua Hu, Michihiro Yasunaga, Richard Lanas Phillips, Irena Gao, et al. Wilds: A benchmark of in-the-wild distribution shifts. In *ICML*, 2021.

[28] Jennifer R Kwapisz, Gary M Weiss, and Samuel A Moore. Activity recognition using cell phone accelerometers. *ACM SIGKDD Explorations Newsletter*, 2011.

[29] Qiao Liu and Hui Xue. Adversarial spectral kernel matching for unsupervised time series domain adaptation. In *IJCAI*, 2021.

[30] Mingsheng Long, Zhangjie Cao, Jianmin Wang, and Michael I Jordan. Conditional adversarial domain adaptation. *NeurIPS*, 2018.

[31] Mostafa Neo Mohsenvand, Mohammad Rasool Izadi, and Pattie Maes. Contrastive representation learning for electroencephalogram classification. In *Machine Learning for Healthcare*. PMLR, 2020.

[32] Bret Nestor, Matthew BA McDermott, Willie Boag, Gabriela Berner, Tristan Naumann, Michael C Hughes, Anna Goldenberg, and Marzyeh Ghassemi. Feature robustness in non-stationary health records: Caveats to deployable model performance in common clinical machine learning tasks. In *Machine Learning for Healthcare*. PMLR, 2019.

[33] Aaron van den Oord, Yazhe Li, and Oriol Vinyals. Representation learning with contrastive predictive coding. *arXiv preprint arXiv:1807.03748*, 2018.

[34] Yilmazcan Ozyurt, Mathias Kraus, Tobias Hatt, and Stefan Feuerriegel. Attdmm: an attentive deep markov model for risk scoring in intensive care units. In *KDD*, 2021.

[35] Zhongyi Pei, Zhangjie Cao, Mingsheng Long, and Jianmin Wang. Multi-adversarial domain adaptation. In *AAAI*, 2018.

[36] Sanjay Purushotham, Wilka Carvalho, Tanachat Nilanon, and Yan Liu. Variational recurrent adversarial deep domain adaptation. In *ICLR*, 2017.

[37] Sanjay Purushotham, Chuizheng Meng, Zhengping Che, and Yan Liu. Benchmarking deep learning models on large healthcare datasets. *Journal of Biomedical Informatics*, 2018.

[38] Mohammad Mahfujur Rahman, Clinton Fookes, Mahsa Baktashmotagh, and Sridha Sridharan. On minimum discrepancy estimation for deep domain adaptation. In *Domain Adaptation for Visual Understanding*, pages 81–94. 2020.

[39] Kendrick Shen, Robbie M Jones, Ananya Kumar, Sang Michael Xie, Jeff Z HaoChen, Tengyu Ma, and Percy Liang. Connect, not collapse: Explaining contrastive learning for unsupervised domain adaptation. In *ICML*, 2022.

[40] Rui Shu, Hung H Bui, Hirokazu Narui, and Stefano Ermon. A dirt-t approach to unsupervised domain adaptation. In *ICLR*, 2018.

[41] Ankit Singh. Clda: Contrastive learning for semi-supervised domain adaptation. *NeurIPS*, 2021.

[42] Allan Stisen, Henrik Blunck, Sourav Bhattacharya, Thor Siiger Prentow, Mikkel Baun Kjærgaard, Anind Dey, Tobias Sonne, and Mads Møller Jensen. Smart devices are different: Assessing and mitigating mobile sensing heterogeneities for activity recognition. In *SenSys*, 2015.

[43] Baochen Sun and Kate Saenko. Deep coral: Correlation alignment for deep domain adaptation. In *ECCV*, 2016.

[44] Shixiang Tang, Peng Su, Dapeng Chen, and Wanli Ouyang. Gradient regularized contrastive learning for continual domain adaptation. In *AAAI*, 2021.

[45] Patrick J Thoral, Jan M Peppink, Ronald H Driessens, Eric JG Sijbrands, Erwin JO Kompanje, Lewis Kaplan, Heatherlee Bailey, Jozef Kesecioglu, Maurizio Cecconi, Matthew Churpek, et al. Sharing icu patient data responsibly under the society of critical care medicine/european society of intensive care medicine joint data science collaboration: the amsterdam university medical centers database (amsterdamumcdb) example. *Critical Care Medicine*, 2021.

[46] Yonglong Tian, Dilip Krishnan, and Phillip Isola. Contrastive multiview coding. In *ECCV*, 2020.

[47] Yonglong Tian, Chen Sun, Ben Poole, Dilip Krishnan, Cordelia Schmid, and Phillip Isola. What makes for good views for contrastive learning? *NeurIPS*, 2020.

[48] Sana Tonekaboni, Danny Eytan, and Anna Goldenberg. Unsupervised representation learning for time series with temporal neighborhood coding. *ICLR*, 2021.

[49] Eric Tzeng, Judy Hoffman, Ning Zhang, Kate Saenko, and Trevor Darrell. Deep domain confusion: Maximizing for domain invariance. *arXiv preprint arXiv:1412.3474*, 2014.

[50] Eric Tzeng, Judy Hoffman, Kate Saenko, and Trevor Darrell. Adversarial discriminative domain adaptation. In *CVPR*, 2017.

[51] Garrett Wilson, Janardhan Rao Doppa, and Diane J Cook. Multi-source deep domain adaptation with weak supervision for time-series sensor data. In *KDD*, 2020.

[52] Garrett Wilson, Janardhan Rao Doppa, and Diane J Cook. Calda: Improving multi-source time series domain adaptation with contrastive adversarial learning. *arXiv preprint arXiv:2109.14778*, 2021.

[53] Minghao Xu, Jian Zhang, Bingbing Ni, Teng Li, Chengjie Wang, Qi Tian, and Wenjun Zhang. Adversarial domain adaptation with domain mixup. In *AAAI*, 2020.

[54] Ling Yang and Shenda Hong. Unsupervised time-series representation learning with iterative bilinear temporal-spectral fusion. In *ICML*, 2022.

[55] Hugo Yèche, Gideon Dresdner, Francesco Locatello, Matthias Hüser, and Gunnar Rätsch. Neighborhood contrastive learning applied to online patient monitoring. In *ICML*, 2021.

[56] Zhihan Yue, Yujing Wang, Juanyong Duan, Tianmeng Yang, Congrui Huang, Yunhai Tong, and Bixiong Xu. Ts2vec: Towards universal representation of time series. In *AAAI*, 2022.

[57] John R Zech, Marcus A Badgeley, Manway Liu, Anthony B Costa, Joseph J Titano, and Eric Karl Oermann. Variable generalization performance of a deep learning model to detect pneumonia in chest radiographs: a cross-sectional study. *PLoS Medicine*, 15(11), 2018.

[58] Xiang Zhang, Ziyuan Zhao, Theodoros Tsiligkaridis, and Marinka Zitnik. Self-supervised contrastive pre-training for time series via time-frequency consistency. *NeurIPS*, 2022.

[59] Yongchun Zhu, Fuzhen Zhuang, Jindong Wang, Guolin Ke, Jingwu Chen, Jiang Bian, Hui Xiong, and Qing He. Deep subdomain adaptation network for image classification. *IEEE Transactions on Neural Networks and Learning Systems*, 2020.

A Related Work

Contrastive Learning: Several methods for contrastive learning have been developed so far. For example, contrastive predictive coding (CPC) [33] predicts the next latent variable in contrast to negative samples from its proposal distribution. SimCLR stands for simple framework for CL of visual representations [8]. It maximizes the agreement between the embeddings of the two augmented views of the same sample and treats all the other samples in the same batch as negative samples. Nearest-neighbor CL (NNCL) [12] creates positive pairs from other samples in the dataset. For this, it takes the embedding of first augmented view and finds its nearest neighbor from the support set. Moment contrast (MoCo) [21] refers to the embeddings of two augmented views as query and key, and then constructs positive pairs for the sample as follows: Key embeddings are generated by a momentum encoder and stored in a queue (whose size is larger than the batch size), while all key embeddings are further used to construct negative pairs for the other sample. Thereby, MoCo generates more negative pairs than the batch size as compared to SimCLR, which is often more efficient in practice.

Contrastive learning for time series: Contrastive learning has been used for time series to learn contextual representation of time series in unsupervised settings. As a result, several methods emerged: Scalable representation learning (SRL) [14], neighborhood contrastive learning (NCL) [55], TS2Vec [56], and temporal neighborhood coding (TNC) [48] treat the neighboring windows of the time series as positive pairs and use other windows to construct negative pairs. For this, SRL, NCL, and TS2Vec minimize the triplet loss, contrastive loss, and hierarchical contrastive loss, respectively, while TNC trains a discriminator network to predict neighborhood information.

There are also more specialized methods. For example, contrastive learning of cardiac signals (CLOCKS) [26] leverages spatial invariance and constructs positive pairs from measurements of the different sensors of the same subject. Temporal and contextual contrasting (TS-TCC) [13] is a variant of CPC and maximizes the agreement between strong and weak augmentations of the same sample in an autoregressive model. Bilinear temporal-spectral fusion (BTSF) [54] constructs the positive pairs via dropout layer applied to the same sample twice and it minimizes a triplet loss for the temporal and spectral features. Time-Frequency Consistency (TF-C) [58] maximizes the agreement between time and frequency embeddings of the same sample.

B Dataset Details

B.1 Benchmark Datasets

We select three sensor datasets that are most commonly used in the earlier works. In each dataset, participants perform various actions while wearing smartphone and/or smartwatches. Based on the sensor measurements, the task is to predict which action the participant is performing. Table 3 provides summary statistics for all datasets. Below, we provide additional information about each dataset.

WISDM. The dataset contains 3-axis accelerometer measurements from 30 participants. The measurements are collected at 20 Hz, and we use non-overlapping segments of 128 time steps to predict the type of the activity of a participant. There are 6 types of activities: walking, jogging, sitting, standing, walking upstairs and walking downstairs. This dataset is particularly challenging due to class imbalance across participants, i.e., there are some participants who did not perform all the activities.

HAR. The dataset contains the measurements of 3-axis accelerometer, 3-axis gyroscope, and 3-axis body acceleration from 30 participants. The measurements are collected at 50 Hz, and we use non-overlapping segments of 128 time steps to predict the type of the activity of a participant. There are 6 types of activities: walking, walking upstairs, walking downstairs, sitting, standing, and lying down.

HHAR. The dataset contains 3-axis accelerometer measurements from 30 participants. The measurements are collected at 50 Hz, and we use non-overlapping segments of 128 time steps to predict the type of the activity of a participant. There are 6 types of activities: biking, sitting, standing, walking, walking upstairs, and walking downstairs.

Table 3: Summary of the sensor datasets.

	#Subjects	#Channels	Length	# Classes	# Training samples	# Val. samples	# Test samples
WISDM	30	3	128	6	3870	1043	1052
HAR	30	9	128	6	7194	1542	1563
HHAR	9	3	128	6	10336	2214	2222

B.2 Medical Datasets

Table 4 shows the summary statistics of both medical datasets MIMIC and AUMC.

Table 5 provides additional details for both datasets MIMIC and AUMC. Both comprise of 41 separate time series, which are then used to predict the outcomes of interest – i.e., decompensation, mortality, and length of stay – via unsupervised domain adaptation.

Table 6 shows the number of patients and the number of samples for each split and each dataset. As a reminder, since we start making the prediction at four hours after the ICU admission, the same patient yields multiple samples when training/testing the models.

Pre-processing: We split the patients of each dataset into 3 parts for training/validation/testing (ratio: 70/15/15). We used a stratified split based on the mortality label. We proceeded analogous to previous works for pre-processing [5, 6, 18, 20, 34, 36, 37, 55]. Each measurement was sampled to hourly resolution, and missing measurements were filled with forward-filling imputation. We applied standard scaling to each measurement based on the statistics from training set. The remaining missing measurements were filled with zero, which corresponds to mean imputation after scaling. We followed best practices in benchmarking data from intensive care units [20, 37]. That is, for each of

Table 4: Summary of datasets.

Name	From	#Patients	#Measurements	Avg. ICU stay (hours)	Mortality (%)
MIMIC	US	49,351	41	72.21	9.95
AUMC	Europe	19,840	41	100.13	8.62

Table 5: Descriptions of medical time series and their summary statistics for MIMIC and AUMC

Measurement	Unit	MIMIC		AUMC	
		Mean	Std. Dev.	Mean	Std. Dev.
Albumin	g/dL	3.053	0.697	2.121	0.575
Alkaline phosphatase	IU/L	115.384	36.044	146.459	49.948
Alanine aminotransferase	IU/L	110.340	98.699	100.352	89.697
Aspartate aminotransferase	IU/L	142.194	160.053	115.663	131.497
Base excess	mEq/L	0.691	1.744	1.291	1.740
Bicarbonate	mEq/L	24.613	4.815	25.815	4.753
Total bilirubin	mg/dL	2.060	4.815	0.975	2.081
Blood urea nitrogen	mg/dL	28.063	23.073	33.112	24.829
Calcium	mg/dL	8.398	0.746	8.121	0.773
Calcium ionized	mmol/L	1.126	0.086	1.161	0.094
Creatine kinase	IU/L	978.735	1402.472	755.806	1163.575
Chloride	mEq/L	103.881	6.224	107.083	6.796
Creatinine	mg/dL	1.364	1.336	1.214	1.001
Diastolic blood pressure	mmHg	63.513	14.857	62.199	14.037
Endtidal co2	mmHg	35.861	7.658	35.405	8.044
Fraction of inspired oxygen	%	48.213	15.95	43.345	10.106
Glucose	mg/dL	134.981	50.227	134.112	36.688
Hematocrit	%	30.850	5.736	31.108	5.230
Hemoglobin	g/dL	10.178	1.983	10.354	1.740
Heart rate	bpm	85.249	17.935	86.609	18.858
Prothrombin time/inter. norm. ratio	–	1.381	0.616	1.312	0.476
Potassium	mEq/L	4.088	0.552	4.141	0.453
Lactate	mmol/L	1.685	1.207	1.674	1.388
Mean arterial pressure	mmHg	79.481	15.368	84.444	17.149
Magnesium	mg/dL	2.107	0.347	2.160	0.446
Sodium	mEq/L	139.079	5.037	140.119	5.324
Co2 partial pressure	mmHg	41.259	9.551	41.590	8.355
Ph of blood	–	7.401	0.070	7.411	0.069
Phosphate	mg/dL	3.503	1.290	3.514	1.240
Platelet count	K/uL	213.982	127.242	245.261	160.271
O2 partial pressure	mmHg	114.686	62.778	101.140	34.704
Partial thromboplastin time	sec	36.537	18.426	44.364	18.862
Systolic blood pressure	mmHg	121.044	21.61	130.308	27.870
Temperature	C	36.949	0.634	36.600	1.095
White blood cell count	K/uL	12.152	8.583	13.314	7.804
Basophils	%	0.264	0.362	0.227	0.417
Eosinophils	%	1.208	1.996	1.167	1.716
Lymphocytes	%	12.316	10.53	11.311	9.873
Neutrophils	%	78.296	13.358	77.720	12.778
Prothrombine time	sec	15.141	6.262	3.455	43.459
Red blood cell count	m/uL	3.398	0.684	3.578	0.886

Table 6: Number of patients and samples for each dataset and each split

	MIMIC			AUMC		
	Train	Validation	Test	Train	Validation	Test
Number of patients	34,290	7,343	7,353	13,802	2958	2964
Number of samples	2,398,546	513,636	512,454	1,332,390	304,981	287,599

the tasks, we start making the prediction at four hours after the ICU admission. In all our experiments, we used a maximum history length $T = 48$ hours. Shorter sequences were pre-padded by zero.

Tasks: We compare the performance of our framework across 3 different standard tasks from the literature [5, 6, 18, 20, 34, 36, 37]. (1) *Decompensation* prediction refers to predicting whether the patient dies within the next 24 hours. (2) *Mortality* prediction refers to predicting whether the patient dies during his/her ICU stay. (3) *Length of stay* prediction refers to predicting the remaining hours of ICU stay for the given patient. This serves as a proxy of the overall health outcome. The distribution of remaining length of ICU stay contains a heavy tail (see Appendix A), which makes it challenging to model it as a regression task. Therefore, we follow the previous works [20, 37] and divide the range of values into 10 buckets and perform an ordinal multiclass classification.

For each task, we performed unsupervised domain adaptation in both ways: MIMIC (source) \mapsto AUMC (target), and AUMC (source) \mapsto MIMIC (target). Later, we also report the corresponding performance on the test samples from the source dataset (i.e., MIMIC \mapsto MIMIC, and AUMC \mapsto AUMC). This way, we aim to provide insights to what extent the different UDA methods provide a trade-off for the performance in the source vs. target domain. It also be loosely interpreted as a upper bound for the prediction performance.

Performance metrics: We report the following performance metrics. The tasks for predicting (1) *decompensation* and (2) *mortality* are binary classification problems. For these tasks, we compare the area under the receiver operating characteristics curve (AUROC) and area under the precision-recall curve (AUPRC). Results for AUPRC are in the Appendix C due to space limitation. The task of predicting (3) *length of stay* is an ordinal multiclass classification problem. For this, we report Cohen’s linear weighted kappa, which measures the correlation between the predicted and ground-truth classes.

Summary statistics for “length of stay”

Here, we provide additional summary statistics for the distribution of “length of stay”. Figure 6 and Figure 7 show the length of stay distribution of all patients in the MIMIC and AUMC datasets, respectively. Further, Figure 8 and Figure 9 show the remaining length of stay distribution for all samples (i.e., all time windows considered for all patients) in MIMIC and AUMC, respectively. Recall that we divide the values of remaining length of stay into 10 buckets; the corresponding fraction of samples belonging to each bucket is reported in Figure 10.

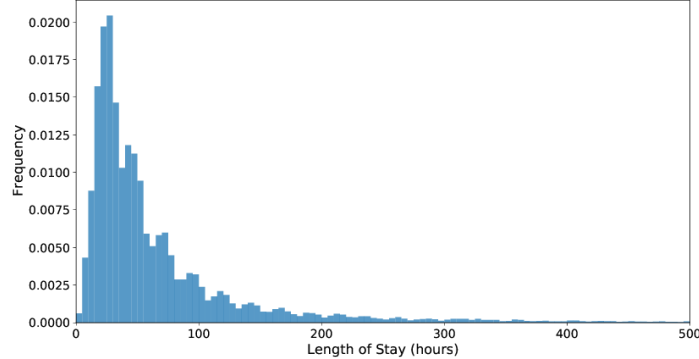


Figure 6: Length of stay distribution of MIMIC patients. For reasons of space, the distribution is cropped at a value of 500.

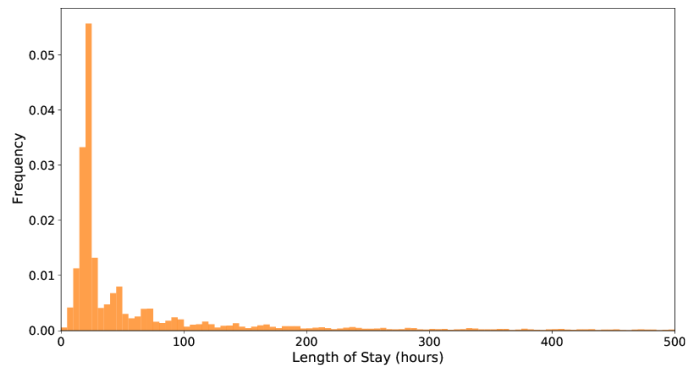


Figure 7: Length of stay distribution of AUMC patients. For reasons of space, the distribution is cropped at a value of 500.

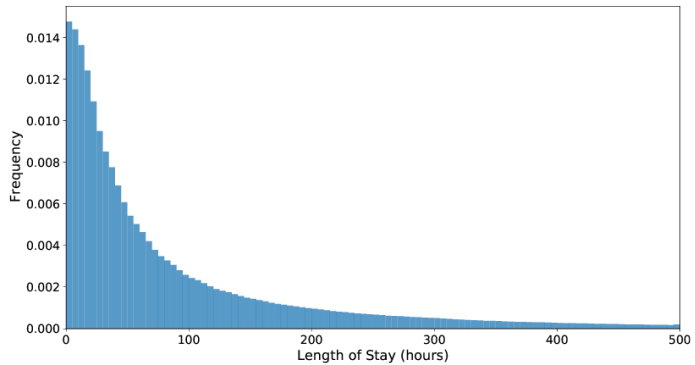


Figure 8: Remaining length of stay distribution of all MIMIC samples. For reasons of space, the distribution is cropped at a value of 500.

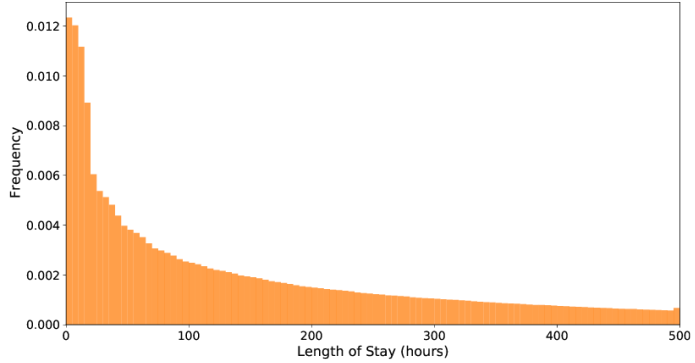


Figure 9: Remaining length of stay distribution of all AUMC samples. For reasons of space, the distribution is cropped at a value of 500.

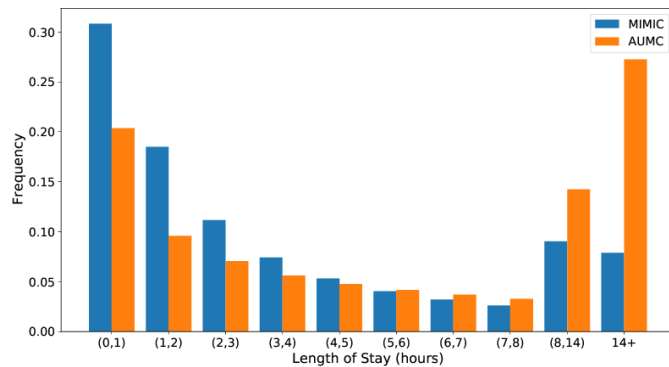


Figure 10: Histogram showing the distribution of remaining length of stay (MIMIC vs. AUMC). The buckets are the following: one bucket for less than one day, one bucket each for days 1 through 7, one bucket for the interval between 7 and 14 days, and one bucket for more than 14 days.

C Training Details

In this section, we provide details on the hyperparameters tuning. Table 7 lists the tuning range of all hyperparameters. To avoid repetition, we list hyperparameters that appear at all methods in the first rows of Table 7. For each dataset (benchmark or medical) and each task (i. e., decompensation, mortality, and length of stay prediction), we performed a grid search for hyperparameter tuning *separately* for each method.

We implemented our CLUDA framework and all the baseline methods in PyTorch. For training and testing, we used NVIDIA GeForce GTX 1080 Ti with 11GB GPU memory. We minimize the loss of each method via Adam optimizer.

We implement the feature extractor $F(\cdot)$ via a temporal convolutional network (TCN) [3]. We set its kernel size 3 and dilation factor 2. For benchmark datasets, we use 6 layers with 16 channels, whereas for medical datasets, we use 5 layers with 64 channels. This configuration remains the same across all methods so that the difference in prediction performance is attributed to their novel UDA approach.

We now explain how we decide the search range of the hyperparameters (e. g., learning rate, weight decay). The low learning rate is preferred so that the methods converge to a certain loss after seeing all samples from each dataset. Especially, the medical dataset MIMIC has roughly 2.4M samples, and it requires $\sim 1.2K$ steps to iterate over all these samples with a batch size of 2048. With higher learning rates, the methods converge to a loss even before one iteration over the dataset. We observed that this leads to suboptimal prediction performance (i.e., lower AUROC, AUPRC and KAPPA scores). For the hyperparameters regarding the contrastive learning framework, we are informed by the configuration of MoCo[21] as a starting point. We explored a certain range to improve the performance. For the feature extractor $F(\cdot)$ and the classifier $C(\cdot)$, we used the best hyperparameter configuration obtained by w/o UDA as a starting point. For benchmark datasets, we trained all methods for max. 5,000 training steps with a batch size of 128. For medical datasets, we trained all methods for max. 30,000 training steps with a batch size of 2048 (except AdvSKM, DDC, DSAN, and MMA with a batch size of 1024 to fit into GPU). We applied early stopping based on the method performance on validation set without the labels from the target domain. To report the test performance of each method with the error bars, we repeated each experiment with 10 different random seeds (i. e., 10 different random initializations).

Here, we compare the runtimes of each method. For this, we use MIMIC-III (the largest dataset in our experiments). We report average runtimes per 100 training steps since the total runtime (i. e., total number of training steps) varies with the step of early stopping applied at each run. For each method, the average runtimes (per 100 training steps) are the following: 44.83 seconds for **w/o UDA**, 122.81 seconds for **VRADA**, 81.06 seconds for **CoDATS**, 151.20 seconds for **TS-SASA**, 73.67 seconds for **AdvSKM with a half batch size**, 119.42 seconds for **CAN**, 83.93 seconds for **CDAN**, 59.92 seconds for **DDC with a half batch size**, 85.67 seconds for **DeepCORAL**, 62.38 seconds for **DSAN with a half batch size**, 83.81 seconds for **HoMM**, 68.92 seconds for **MMDA with a half batch size**, and 96.11 seconds for our **CLUDA**.

Augmentations

To capture the contextual representation of medical time series, we apply semantic-preserving augmentations [10, 26, 55] in our CLUDA framework. We list the augmentations and their optimal hyperparameters (search range in parenthesis) below:

History crop: We mask out a minimum 20 % (10 % – 40 %) of the initial time series with 50 % (20 % – 50 %) probability.

History cutout: We mask out a random 15 % time-window (5 % – 20 %) of time series with 50 % (20 % – 70 %) probability.

Channel dropout: We mask out each channel (i. e., type of measurement) independently with 10 % (5 % – 30 %) probability.

Gaussian noise: We apply Gaussian noise to each measurement independently with standard deviation of 0.1 (0.05 – 0.2).

We apply these augmentations sequentially to each time series twice. As a result, we have two semantic-preserving augmented views of the same time series for our CLUDA framework. Of note, we trained all the baseline methods with and without the augmentations of time series. We always report the their best results.

Table 7: Hyperparameter tuning.

Method	Hyperparameter	Tuning Range
All methods, w/o UDA	Classifier hidden dim.	64, 128, 256
	Batch normalization	True, False
	Dropout	0, 0.1, 0.2
	Learning rate	$5 \cdot 10^{-5}, 2 \cdot 10^{-4}, 5 \cdot 10^{-4}$
	Weight decay	$1 \cdot 10^{-4}, 1 \cdot 10^{-3}, 1 \cdot 10^{-4}$
VRADA[36]	VRNN hidden dim.	32, 62, 128
	VRNN latent dim.	32, 64, 128
	VRNN num. layers	1, 2, 3
	Discriminator hidden dim.	64, 128, 256
	Weight discriminator loss	0.1, 0.5, 1
	Weight KL divergence	0.1, 0.5, 1
CoDATS[51]	Weight neg. log-likelihood	0.1, 0.5, 1
	Discriminator hidden dim.	64, 128, 256
TS-SASA[5]	Weight discriminator loss	0.1, 0.5, 1
	LSTM hidden dim	4, 8, 12
	Num. segments	4, 8, 12, 24
	Segment lengths	3, 6, 12, 24
	MMD kernel type	Linear, Gaussian
	Weight intra-attention loss	0.1, 0.5, 1
AdvSKM[29]	Weight inter-attention loss	0.1, 0.5, 1
	Spectral kernel hidden dim.	32, 64, 128
	Spectral kernel output dim.	32, 64, 128
	Spectral kernel type	Linear, Gaussian
	Num. kernel (if Gaussian)	3, 5, 7
CAN[25]	Weight MMD loss	0.1, 0.5, 1
	Kernel type	Linear, Gaussian
	Num. kernel (if Gaussian)	1, 3, 5, 7
	Num. iterations k-means clustering (each loop)	1,3,5
	Sampling type	Random, Class-aware
CDAN[30]	Weight MMD loss	0.1, 0.5, 1
	Discriminator hidden dim.	64, 128, 256
	Multiplier discriminator update	0.1, 1, 10
	Weight discriminator loss	0.1, 0.5, 1
DDC[49]	Weight conditional entropy loss	0.1, 0.5, 1
	Kernel type	Linear, Gaussian
	Num. kernel (if Gaussian)	1, 3, 5, 7
DeepCORAL[43]	Weight MMD loss	0.1, 0.5, 1
	Weight CORAL loss	0.1, 0.3, 0.5, 1
DSAN[59]	Kernel multiplier	1, 2, 3
	Num. kernel	3, 5, 7
	Weight domain loss	0.1, 0.5, 1
HoMM[7]	Moment order	1, 2, 3
	Weight domain discrepancy loss	0.1, 0.5, 1
	Weight discriminative clustering loss	0.1, 0.5, 1
MMDA[38]	Kernel type	Linear, Gaussian
	Num. kernel (if Gaussian)	1, 3, 5, 7
	Weight MMD loss	0.1, 0.5, 1
	Weight CORAL loss	0.1, 0.5, 1
	Weight Entropy loss	0.1, 0.5, 1
CLUDA (ours)	Momentum	0.9, 0.95, 0.99
	Queue size	24576, 49152, 98304
	Discriminator hidden dim.	64, 128, 256
	Projector hidden dim.	64, 128, 256
	λ_{disc}	0.1, 0.5, 1
	λ_{CL}	0.05, 0.1, 0.2
	λ_{NNCL}	0.05, 0.1, 0.2

D UDA on Benchmark Datasets

We perform the activity prediction as a UDA task based on the benchmark datasets WISDM, HAR, and HHAR. For each dataset, we present the prediction results for 10 randomly selected source-target pairs. For each source-target pair, we repeat the experiments with 10 random initializations and report the mean values. Table 8 shows the accuracy on the target domains and average accuracy for each dataset. Similarly, Table 9 shows the Macro-F1 on the target domains and average Macro-F1 for each dataset.

Table 8: Activity prediction for each dataset between various subjects. Shown: mean Accuracy over 10 random initializations.

Sour \mapsto Tar	w/o UDA	VRADA	CoDATS	AdvSKM	CAN	CDAN	DDC	DeepCORAL	DSAN	HoMM	MMDA	CLUDA (ours)
WISDM 12 \mapsto 19	0.745	0.558	0.633	0.639	0.594	0.488	0.564	0.433	0.639	0.415	0.358	0.694
WISDM 12 \mapsto 7	0.654	0.708	0.721	0.742	0.588	0.771	0.692	0.592	0.625	0.546	0.679	0.792
WISDM 18 \mapsto 20	0.385	0.571	0.634	0.390	0.439	0.771	0.390	0.380	0.366	0.429	0.380	0.780
WISDM 19 \mapsto 2	0.410	0.644	0.395	0.434	0.322	0.346	0.459	0.473	0.366	0.488	0.385	0.561
WISDM 2 \mapsto 28	0.787	0.729	0.809	0.809	0.760	0.813	0.782	0.827	0.773	0.787	0.813	0.849
WISDM 26 \mapsto 2	0.634	0.683	0.727	0.620	0.580	0.615	0.600	0.737	0.605	0.702	0.634	0.863
WISDM 28 \mapsto 2	0.702	0.688	0.717	0.707	0.561	0.580	0.702	0.649	0.673	0.644	0.668	0.741
WISDM 28 \mapsto 20	0.727	0.741	0.741	0.707	0.673	0.776	0.727	0.737	0.746	0.790	0.722	0.820
WISDM 7 \mapsto 2	0.620	0.605	0.610	0.610	0.571	0.649	0.620	0.624	0.620	0.605	0.605	0.712
WISDM 7 \mapsto 26	0.722	0.693	0.702	0.702	0.717	0.722	0.717	0.683	0.698	0.698	0.712	0.727
WISDM Avg	0.639	0.662	0.669	0.636	0.580	0.653	0.625	0.613	0.611	0.610	0.596	0.754
HAR 15 \mapsto 19	0.722	0.756	0.733	0.741	0.685	0.759	0.733	0.759	0.874	0.748	0.726	0.967
HAR 18 \mapsto 21	0.552	0.794	0.552	0.555	0.552	0.803	0.548	0.610	0.558	0.581	0.555	0.910
HAR 19 \mapsto 25	0.461	0.768	0.468	0.452	0.661	0.771	0.455	0.590	0.774	0.487	0.448	0.932
HAR 19 \mapsto 27	0.751	0.793	0.709	0.723	0.782	0.807	0.747	0.744	0.891	0.726	0.754	0.996
HAR 20 \mapsto 6	0.616	0.808	0.661	0.641	0.747	0.820	0.608	0.686	0.784	0.673	0.694	1.000
HAR 23 \mapsto 13	0.448	0.736	0.504	0.504	0.476	0.700	0.504	0.668	0.628	0.604	0.572	0.788
HAR 24 \mapsto 22	0.808	0.837	0.820	0.833	0.820	0.837	0.808	0.743	0.808	0.853	0.829	0.988
HAR 25 \mapsto 24	0.545	0.817	0.583	0.566	0.721	0.790	0.593	0.648	0.883	0.607	0.666	0.993
HAR 3 \mapsto 20	0.852	0.752	0.874	0.878	0.652	0.815	0.885	0.848	0.804	0.874	0.815	0.967
HAR 13 \mapsto 19	0.796	0.752	0.793	0.807	0.785	0.841	0.800	0.793	0.726	0.815	0.800	0.904
HAR Avg	0.655	0.781	0.670	0.670	0.688	0.794	0.668	0.709	0.773	0.697	0.686	0.944
HHAR 0 \mapsto 2	0.656	0.593	0.650	0.681	0.721	0.676	0.659	0.618	0.292	0.680	0.671	0.726
HHAR 1 \mapsto 6	0.673	0.690	0.686	0.652	0.619	0.717	0.672	0.712	0.689	0.725	0.686	0.855
HHAR 2 \mapsto 4	0.296	0.476	0.381	0.291	0.391	0.472	0.304	0.332	0.229	0.332	0.238	0.585
HHAR 4 \mapsto 0	0.183	0.263	0.229	0.203	0.194	0.262	0.216	0.259	0.193	0.193	0.205	0.353
HHAR 4 \mapsto 1	0.454	0.558	0.501	0.494	0.549	0.690	0.502	0.482	0.504	0.628	0.551	0.774
HHAR 5 \mapsto 1	0.757	0.775	0.761	0.737	0.829	0.857	0.744	0.787	0.407	0.784	0.790	0.948
HHAR 7 \mapsto 1	0.358	0.575	0.551	0.426	0.534	0.413	0.378	0.511	0.366	0.496	0.415	0.875
HHAR 7 \mapsto 5	0.199	0.523	0.380	0.192	0.592	0.492	0.229	0.489	0.233	0.328	0.320	0.636
HHAR 8 \mapsto 3	0.760	0.813	0.766	0.748	0.860	0.942	0.763	0.869	0.602	0.844	0.934	0.942
HHAR 8 \mapsto 4	0.627	0.720	0.601	0.650	0.660	0.712	0.629	0.618	0.516	0.658	0.701	0.896
HHAR Avg	0.496	0.599	0.551	0.508	0.595	0.623	0.510	0.568	0.403	0.567	0.551	0.759

Higher is better. Best value in bold.

Overall, our CLUDA outperforms the UDA baselines by a large margin, as discussed in the main paper. Specifically, CLUDA achieves the best accuracy in 28 out of 30 UDA scenarios and the best Macro-F1 in 27 out of 30 UDA scenarios. Thereby, the results confirm the effectiveness of our method.

Table 9: Activity prediction for each dataset between various subjects. Shown: mean MacroF1 over 10 random initializations.

Sour \mapsto Tar	w/o UDA	VRADA	CoDATS	AdvSKM	CAN	CDAN	DDC	DeepCORAL	DSAN	HomM	MMDA	CLUDA (ours)
WISDM 12 \mapsto 19	0.577	0.410	0.456	0.510	0.508	0.298	0.396	0.317	0.518	0.281	0.233	0.532
WISDM 12 \mapsto 7	0.543	0.437	0.612	0.655	0.636	0.546	0.632	0.486	0.574	0.442	0.539	0.678
WISDM 18 \mapsto 20	0.339	0.578	0.427	0.348	0.389	0.600	0.383	0.379	0.268	0.421	0.280	0.673
WISDM 19 \mapsto 2	0.436	0.615	0.403	0.460	0.327	0.312	0.459	0.501	0.428	0.522	0.306	0.458
WISDM 2 \mapsto 28	0.696	0.688	0.688	0.742	0.610	0.644	0.669	0.726	0.654	0.691	0.677	0.788
WISDM 26 \mapsto 2	0.472	0.517	0.598	0.463	0.362	0.404	0.414	0.618	0.424	0.519	0.453	0.701
WISDM 28 \mapsto 2	0.450	0.473	0.492	0.484	0.412	0.400	0.484	0.495	0.451	0.511	0.430	0.710
WISDM 28 \mapsto 20	0.560	0.672	0.578	0.557	0.655	0.605	0.571	0.620	0.615	0.699	0.537	0.703
WISDM 7 \mapsto 2	0.443	0.399	0.494	0.476	0.490	0.543	0.496	0.490	0.481	0.494	0.459	0.576
WISDM 7 \mapsto 26	0.407	0.308	0.405	0.416	0.395	0.344	0.412	0.396	0.401	0.406	0.385	0.403
WISDM Avg	0.492	0.510	0.515	0.511	0.479	0.469	0.492	0.503	0.482	0.498	0.430	0.622
HAR 15 \mapsto 19	0.647	0.657	0.663	0.664	0.593	0.696	0.658	0.708	0.831	0.686	0.656	0.957
HAR 18 \mapsto 21	0.431	0.668	0.428	0.445	0.434	0.718	0.427	0.539	0.458	0.486	0.440	0.923
HAR 19 \mapsto 25	0.369	0.737	0.381	0.359	0.640	0.768	0.360	0.535	0.754	0.397	0.348	0.932
HAR 19 \mapsto 27	0.685	0.723	0.643	0.652	0.723	0.752	0.683	0.689	0.852	0.650	0.684	0.996
HAR 20 \mapsto 6	0.539	0.773	0.603	0.576	0.725	0.796	0.529	0.666	0.759	0.627	0.641	1.000
HAR 23 \mapsto 13	0.377	0.696	0.440	0.436	0.410	0.660	0.447	0.616	0.606	0.549	0.527	0.762
HAR 24 \mapsto 22	0.712	0.749	0.714	0.726	0.772	0.756	0.710	0.647	0.726	0.768	0.722	0.983
HAR 25 \mapsto 24	0.488	0.782	0.516	0.503	0.702	0.765	0.527	0.625	0.873	0.538	0.641	0.992
HAR 3 \mapsto 20	0.813	0.671	0.853	0.847	0.549	0.769	0.852	0.828	0.757	0.860	0.784	0.968
HAR 13 \mapsto 19	0.743	0.696	0.738	0.769	0.729	0.837	0.752	0.763	0.662	0.798	0.752	0.911
HAR Avg	0.580	0.715	0.598	0.598	0.628	0.752	0.595	0.662	0.728	0.636	0.619	0.942
HHAR 0 \mapsto 2	0.606	0.536	0.598	0.628	0.667	0.611	0.605	0.569	0.205	0.627	0.612	0.710
HHAR 1 \mapsto 6	0.685	0.702	0.696	0.662	0.621	0.727	0.678	0.725	0.696	0.726	0.693	0.858
HHAR 2 \mapsto 4	0.196	0.415	0.320	0.219	0.294	0.431	0.231	0.305	0.143	0.230	0.192	0.526
HHAR 4 \mapsto 0	0.147	0.243	0.222	0.163	0.165	0.273	0.175	0.249	0.116	0.179	0.162	0.352
HHAR 4 \mapsto 1	0.415	0.545	0.469	0.466	0.523	0.667	0.456	0.461	0.488	0.607	0.517	0.751
HHAR 5 \mapsto 1	0.711	0.756	0.723	0.692	0.813	0.848	0.707	0.766	0.285	0.738	0.765	0.950
HHAR 7 \mapsto 1	0.275	0.583	0.528	0.338	0.524	0.412	0.280	0.483	0.278	0.461	0.367	0.875
HHAR 7 \mapsto 5	0.151	0.529	0.374	0.154	0.546	0.480	0.175	0.496	0.192	0.323	0.283	0.626
HHAR 8 \mapsto 3	0.701	0.818	0.734	0.692	0.845	0.943	0.719	0.872	0.564	0.836	0.936	0.944
HHAR 8 \mapsto 4	0.542	0.715	0.539	0.580	0.596	0.710	0.550	0.578	0.434	0.606	0.636	0.891
HHAR Avg	0.443	0.584	0.520	0.459	0.559	0.610	0.458	0.550	0.340	0.533	0.516	0.748

Higher is better. Best value in bold.

E Embedding Visualization

In this section, we provide the t-SNE visualization (see Fig. 11) for the embeddings of each method from HHAR dataset. When there is no domain adaptation (see Fig. 11a of w/o UDA), there is a significant domain shift between source and target. As a result, embeddings of one class in target domain overlap with embeddings of another class in source domain. Thereby, the classifier learned on the source domain cannot generalize well over the target domain. The UDA baselines mitigate the domain shift; however, they still mix several classes. On the other hand, our CLUDA clearly pulls the embeddings of the same class (even though they are in different domains), and facilitates better generalization in the target domain.

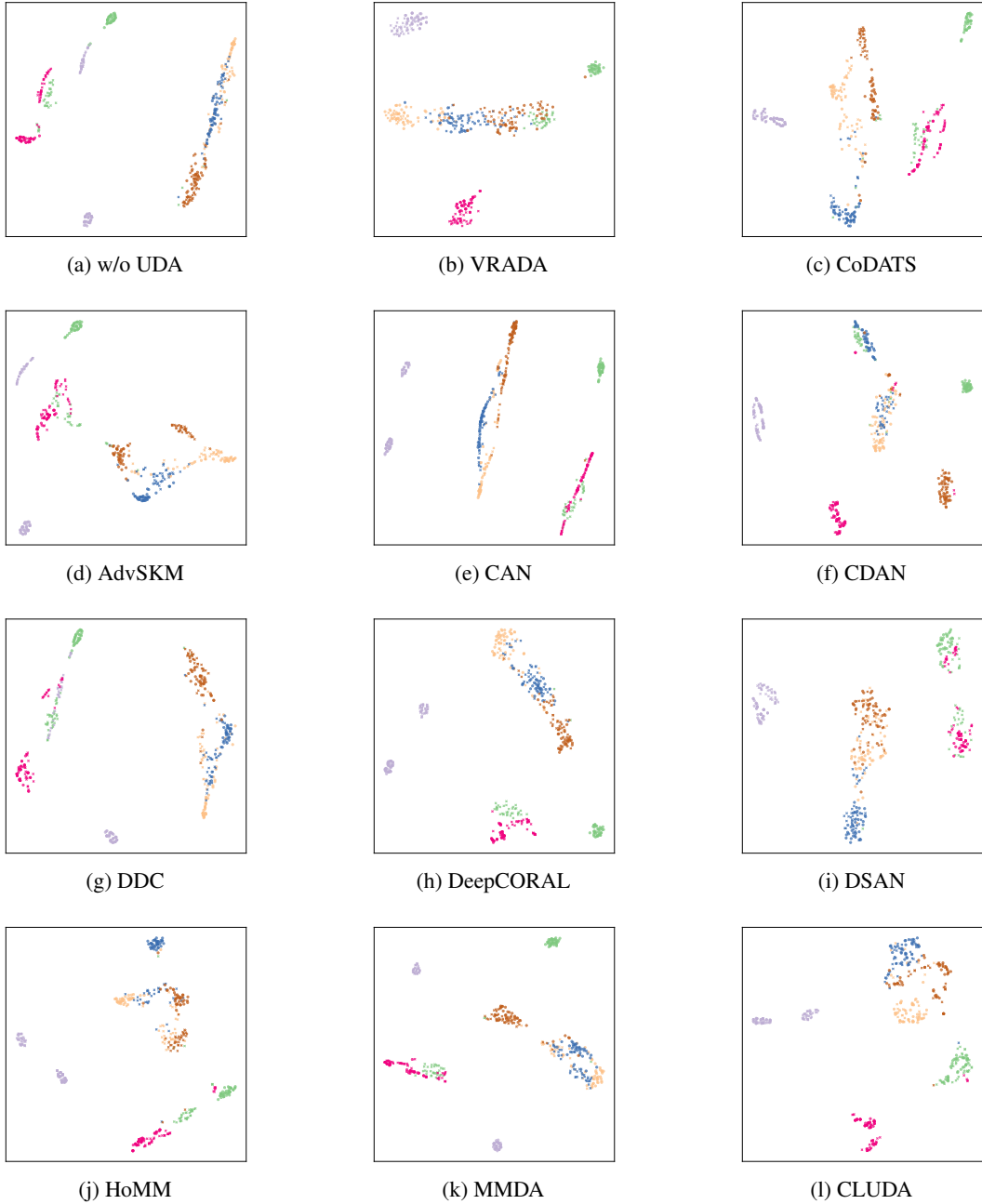


Figure 11: t-SNE visualization of the embeddings from each model on HHAR dataset. Each class is represented by a different color. Shape shows source and target domains (circle vs. cross).

F Ablation Study for UDA on Benchmark Datasets

We further conduct an ablation study on the benchmark datasets WISDM, HAR, and HHAR. We use the same variants of CLUDA from the main paper (see Sec. 6.1: **w/o CL and w/o NNCL**, **w/o CL, w/o NNCL**, and **w/o Discriminator**). Similar to the main experiments, for each dataset, we present the prediction results for 10 randomly selected source-target pairs. For each source-target pair, we repeat the experiments with 10 random initializations and report the mean values. Table 10 shows the accuracy on the target domains and average accuracy for each dataset. Similarly, Table 11 shows the Macro-F1 on the target domains and average Macro-F1 for each dataset.

Table 10: Activity prediction for each dataset between various subjects. Shown: mean Accuracy over 10 random initializations.

Sour \mapsto Tar	w/o UDA	w/o CL and w/o NNCL	w/o CL	w/o NNCL	w/o Discriminator	CLUDA (ours)
WISDM 12 \mapsto 19	0.745	0.433	0.770	0.470	0.803	0.694
WISDM 12 \mapsto 7	0.654	0.583	0.542	0.700	0.700	0.792
WISDM 18 \mapsto 20	0.385	0.595	0.473	0.717	0.463	0.780
WISDM 19 \mapsto 2	0.410	0.410	0.463	0.517	0.527	0.561
WISDM 2 \mapsto 28	0.787	0.729	0.716	0.707	0.747	0.849
WISDM 26 \mapsto 2	0.634	0.654	0.693	0.810	0.824	0.863
WISDM 28 \mapsto 2	0.702	0.337	0.507	0.522	0.761	0.741
WISDM 28 \mapsto 20	0.727	0.780	0.673	0.771	0.795	0.820
WISDM 7 \mapsto 2	0.620	0.634	0.659	0.688	0.741	0.712
WISDM 7 \mapsto 26	0.722	0.707	0.707	0.678	0.707	0.727
WISDM Avg	0.639	0.586	0.620	0.658	0.707	0.754
HAR 15 \mapsto 19	0.722	0.793	0.711	0.804	0.807	0.967
HAR 18 \mapsto 21	0.552	0.813	0.806	0.855	0.861	0.910
HAR 19 \mapsto 25	0.461	0.758	0.652	0.800	0.652	0.932
HAR 19 \mapsto 27	0.751	0.933	0.937	0.944	0.832	0.996
HAR 20 \mapsto 6	0.616	0.959	0.910	0.865	0.906	1.000
HAR 23 \mapsto 13	0.448	0.696	0.680	0.668	0.740	0.788
HAR 24 \mapsto 22	0.808	0.837	0.873	0.918	0.898	0.988
HAR 25 \mapsto 24	0.545	0.938	0.890	0.928	0.910	0.993
HAR 3 \mapsto 20	0.852	0.926	0.800	0.874	0.819	0.967
HAR 13 \mapsto 19	0.796	0.678	0.752	0.759	0.807	0.904
HAR Avg	0.655	0.833	0.801	0.841	0.823	0.944
HHAR 0 \mapsto 2	0.656	0.666	0.677	0.606	0.725	0.726
HHAR 1 \mapsto 6	0.673	0.735	0.731	0.771	0.790	0.855
HHAR 2 \mapsto 4	0.296	0.530	0.393	0.554	0.570	0.585
HHAR 4 \mapsto 0	0.183	0.197	0.210	0.276	0.348	0.353
HHAR 4 \mapsto 1	0.454	0.536	0.711	0.554	0.782	0.774
HHAR 5 \mapsto 1	0.757	0.817	0.887	0.866	0.914	0.948
HHAR 7 \mapsto 1	0.358	0.493	0.660	0.557	0.728	0.875
HHAR 7 \mapsto 5	0.199	0.357	0.460	0.423	0.547	0.636
HHAR 8 \mapsto 3	0.760	0.836	0.821	0.864	0.888	0.942
HHAR 8 \mapsto 4	0.627	0.644	0.555	0.671	0.710	0.896
HHAR Avg	0.496	0.581	0.610	0.614	0.700	0.759

Higher is better. Best value in bold.

Overall, our complete CLUDA outperforms all its variants by a significant margin, which confirms our chosen architecture.

Table 11: Activity prediction for each dataset between various subjects. Shown: mean MacroF1 over 10 random initializations.

Sour \mapsto Tar	w/o UDA	w/o CL and w/o NNCL	w/o CL	w/o NNCL	w/o Discriminator	CLUDA (ours)
WISDM 12 \mapsto 19	0.577	0.334	0.606	0.309	0.620	0.532
WISDM 12 \mapsto 7	0.543	0.458	0.468	0.534	0.525	0.678
WISDM 18 \mapsto 20	0.339	0.485	0.481	0.507	0.523	0.673
WISDM 19 \mapsto 2	0.436	0.358	0.492	0.415	0.565	0.458
WISDM 2 \mapsto 28	0.696	0.669	0.685	0.682	0.667	0.788
WISDM 26 \mapsto 2	0.472	0.367	0.494	0.620	0.642	0.701
WISDM 28 \mapsto 2	0.450	0.373	0.469	0.457	0.638	0.710
WISDM 28 \mapsto 20	0.560	0.652	0.547	0.619	0.686	0.703
WISDM 7 \mapsto 2	0.443	0.418	0.455	0.499	0.556	0.576
WISDM 7 \mapsto 26	0.407	0.321	0.337	0.341	0.343	0.403
WISDM Avg	0.492	0.444	0.503	0.498	0.577	0.622
HAR 15 \mapsto 19	0.647	0.730	0.622	0.783	0.746	0.957
HAR 18 \mapsto 21	0.431	0.746	0.748	0.840	0.835	0.923
HAR 19 \mapsto 25	0.369	0.755	0.564	0.797	0.603	0.932
HAR 19 \mapsto 27	0.685	0.896	0.918	0.922	0.775	0.996
HAR 20 \mapsto 6	0.539	0.961	0.900	0.855	0.912	1.000
HAR 23 \mapsto 13	0.377	0.670	0.607	0.638	0.687	0.762
HAR 24 \mapsto 22	0.712	0.797	0.798	0.883	0.848	0.983
HAR 25 \mapsto 24	0.488	0.926	0.861	0.917	0.899	0.992
HAR 3 \mapsto 20	0.813	0.920	0.713	0.835	0.740	0.968
HAR 13 \mapsto 19	0.743	0.681	0.680	0.777	0.785	0.911
HAR Avg	0.580	0.808	0.741	0.825	0.783	0.942
HHAR 0 \mapsto 2	0.606	0.599	0.611	0.549	0.661	0.710
HHAR 1 \mapsto 6	0.685	0.729	0.721	0.771	0.785	0.858
HHAR 2 \mapsto 4	0.196	0.464	0.272	0.484	0.493	0.526
HHAR 4 \mapsto 0	0.147	0.166	0.188	0.274	0.331	0.352
HHAR 4 \mapsto 1	0.415	0.487	0.652	0.497	0.748	0.751
HHAR 5 \mapsto 1	0.711	0.809	0.877	0.864	0.916	0.950
HHAR 7 \mapsto 1	0.275	0.467	0.626	0.536	0.732	0.875
HHAR 7 \mapsto 5	0.151	0.348	0.410	0.413	0.549	0.626
HHAR 8 \mapsto 3	0.701	0.822	0.809	0.859	0.876	0.944
HHAR 8 \mapsto 4	0.542	0.610	0.479	0.628	0.671	0.891
HHAR Avg	0.443	0.550	0.565	0.588	0.676	0.748

Higher is better. Best value in bold.

G UDA across Various Age Groups

Following the earlier works [36, 5], we conducted extensive experiments to compare the UDA performance of our CLUDA framework across various age groups. We consider the following groups: (1) Group 1: working-age adult (20 to 45 years old patients); (2) Group 2: old working-age adult (46 to 65 years old patients); (3) Group 3: elderly (66 to 85 years old patients); and (4) Group 4: seniors (85+ years old patients). Therefore, within each dataset (MIMIC and AUMC), we list the results of all combinations of Source \mapsto Target for mortality prediction (i. e., Group 1 \mapsto Group 2, Group 1 \mapsto Group 3, ..., Group 4 \mapsto Group 3). Results are shown in Table 1 (in the main paper) for MIMIC and Table 12 for AUMC.

We further extend the experiments to **across datasets**. That means, we pick the source domain as one age group from one dataset (e. g., Group 1 of MIMIC) and pick the target domain as one age group from the other dataset (e. g., Group 3 of AUMC). We, again, conducted the experiments for all combinations of age groups across the datasets. Results are shown in Table 13 from MIMIC to AUMC and Table 14 from AUMC to MIMIC.

We report the mean over 10 random initialization. For better readability, we omitted the standard deviation. Nevertheless, we highlight performance results in bold when corresponding baselines are outperformed at a significant level.

Table 12: Mortality prediction between various age groups of AUMC. Shown: mean AUROC over 10 random initializations.

Sour \mapsto Tar	w/o UDA	VRADA	CoDATS	AdvSKM	CAN	CDAN	DDC	DeepCORAL	DSAN	HoMM	MMDA	CLUDA (ours)
1 \mapsto 2	0.557	0.583	0.545	0.562	0.536	0.551	0.527	0.538	0.502	0.538	0.536	0.571
1 \mapsto 3	0.602	0.659	0.602	0.623	0.670	0.578	0.681	0.669	0.657	0.678	0.659	0.686
1 \mapsto 4	0.683	0.732	0.672	0.702	0.727	0.677	0.738	0.740	0.747	0.739	0.742	0.749
2 \mapsto 1	0.719	0.716	0.728	0.740	0.629	0.658	0.749	0.685	0.701	0.690	0.709	0.743
2 \mapsto 3	0.728	0.743	0.728	0.740	0.705	0.706	0.692	0.705	0.740	0.714	0.688	0.765
2 \mapsto 4	0.795	0.783	0.798	0.800	0.772	0.742	0.775	0.780	0.800	0.784	0.791	0.795
3 \mapsto 1	0.780	0.761	0.778	0.781	0.722	0.636	0.745	0.733	0.732	0.745	0.726	0.812
3 \mapsto 2	0.595	0.618	0.588	0.604	0.575	0.607	0.572	0.576	0.585	0.553	0.550	0.657
3 \mapsto 4	0.817	0.788	0.815	0.832	0.823	0.790	0.809	0.813	0.817	0.794	0.803	0.836
4 \mapsto 1	0.730	0.739	0.727	0.738	0.718	0.671	0.726	0.690	0.683	0.721	0.740	0.731
4 \mapsto 2	0.640	0.618	0.640	0.628	0.563	0.669	0.641	0.583	0.654	0.637	0.502	0.635
4 \mapsto 3	0.709	0.715	0.708	0.717	0.720	0.707	0.689	0.674	0.705	0.721	0.677	0.740
Avg	0.696	0.705	0.694	0.706	0.680	0.666	0.695	0.682	0.694	0.693	0.677	0.727

Higher is better. Best value in bold. Second best results are underlined if stds overlap.

Table 13: Mortality prediction between various age groups from MIMIC to AUMC. Shown: mean AUROC over 10 random initializations.

Sour \mapsto Tar	w/o UDA	VRADA	CoDATS	AdvSKM	CAN	CDAN	DDC	DeepCORAL	DSAN	HoMM	MMDA	CLUDA (ours)
1 \mapsto 1	0.736	0.751	0.731	0.734	0.723	0.754	0.731	0.742	0.720	0.732	0.729	0.782
1 \mapsto 2	0.628	0.721	0.627	0.637	0.689	0.614	0.607	0.636	0.604	0.587	0.611	0.731
1 \mapsto 3	0.662	0.688	0.657	0.671	0.656	0.654	0.618	0.661	0.629	0.630	0.653	0.707
1 \mapsto 4	0.754	0.745	0.753	0.753	0.725	0.745	0.713	0.705	0.711	0.716	0.699	0.754
2 \mapsto 1	0.835	0.760	0.828	0.832	0.810	0.783	0.832	0.826	0.815	0.830	0.825	0.822
2 \mapsto 2	0.629	0.699	0.633	0.635	0.634	0.691	0.631	0.630	0.634	0.633	0.636	0.705
2 \mapsto 3	0.656	0.701	0.667	0.689	0.688	0.655	0.652	0.659	0.676	0.653	0.655	0.714
2 \mapsto 4	0.773	0.764	0.776	0.777	0.761	0.755	0.771	0.771	0.772	0.768	0.757	0.807
3 \mapsto 1	0.763	0.748	0.754	0.776	0.762	0.746	0.764	0.769	0.729	0.753	0.737	0.789
3 \mapsto 2	0.627	0.622	0.615	0.621	0.696	0.672	0.618	0.631	0.634	0.619	0.635	0.691
3 \mapsto 3	0.711	0.701	0.712	0.716	0.706	0.702	0.708	0.712	0.717	0.706	0.719	0.751
3 \mapsto 4	0.782	0.750	0.784	0.785	0.772	0.756	0.784	0.786	0.785	<u>0.788</u>	0.771	0.796
4 \mapsto 1	0.714	0.676	0.697	0.716	0.672	0.689	0.708	0.707	0.631	0.700	0.617	0.689
4 \mapsto 2	0.668	0.666	0.661	0.649	0.626	0.713	0.670	0.643	0.684	0.660	0.658	0.673
4 \mapsto 3	0.619	0.627	0.614	0.606	0.617	0.620	0.616	0.609	0.626	0.613	0.610	0.635
4 \mapsto 4	0.758	0.709	0.757	0.744	0.752	0.748	0.762	0.738	0.760	0.753	0.738	0.768
Avg	0.707	0.708	0.704	0.709	0.706	0.706	0.699	0.702	0.695	0.696	0.691	0.738

Higher is better. Best value in bold. Second best results are underlined if stds overlap.

Table 14: Mortality prediction between various age groups from AUMC to MIMIC. Shown: mean AUROC over 10 random initializations.

Sour \mapsto Tar	w/o UDA	VRADA	CoDATS	AdvSKM	CAN	CDAN	DDC	DeepCORAL	DSAN	HoMM	MMDA	CLUDA (ours)
1 \mapsto 1	0.693	0.733	0.694	0.698	0.738	0.681	0.713	0.714	0.722	0.714	0.708	0.791
1 \mapsto 2	0.665	0.722	0.666	0.696	0.751	0.648	0.746	0.751	0.736	0.756	0.745	0.776
1 \mapsto 3	0.609	0.644	0.609	0.625	0.630	0.594	0.620	0.623	0.623	0.629	0.619	0.679
1 \mapsto 4	0.600	0.579	0.599	0.609	0.584	0.585	0.584	0.593	0.603	0.590	0.551	0.598
2 \mapsto 1	0.703	0.747	0.735	0.727	0.776	0.736	0.640	0.791	0.699	0.697	0.749	0.780
2 \mapsto 2	0.684	0.758	0.697	0.730	0.755	0.757	0.626	0.706	0.742	0.695	0.750	0.771
2 \mapsto 3	0.641	0.693	0.648	0.659	0.664	0.677	0.625	0.675	0.676	0.645	0.637	0.702
2 \mapsto 4	0.592	0.590	0.597	0.573	0.516	0.556	0.591	0.570	0.585	0.578	0.572	0.608
3 \mapsto 1	0.805	0.784	0.794	<u>0.801</u>	0.796	0.778	0.776	0.794	0.738	0.768	0.802	0.785
3 \mapsto 2	0.751	0.769	0.747	0.747	0.732	0.698	0.738	0.746	0.683	0.744	0.743	0.774
3 \mapsto 3	0.720	<u>0.723</u>	0.718	<u>0.722</u>	0.686	0.714	0.699	0.679	0.677	0.695	0.692	0.729
3 \mapsto 4	0.622	0.608	0.615	0.624	0.568	0.598	0.623	0.599	0.622	0.618	0.604	0.615
4 \mapsto 1	0.801	0.756	0.808	0.819	0.796	0.786	0.709	0.831	0.701	0.806	0.734	0.819
4 \mapsto 2	0.750	0.739	0.756	0.761	0.757	0.744	0.695	0.769	0.757	0.752	0.764	0.752
4 \mapsto 3	0.709	0.695	0.710	0.711	0.674	0.697	0.663	0.719	0.671	0.713	0.647	0.711
4 \mapsto 4	<u>0.697</u>	0.664	<u>0.695</u>	0.698	0.645	0.684	0.663	0.641	0.684	0.693	0.643	0.679
Avg	0.690	0.700	0.693	0.700	0.692	0.683	0.669	0.700	0.682	0.693	0.685	0.723

Higher is better. Best value in bold. Second best results are underlined if stds overlap.

Overall, in this section we present 56 prediction tasks to compare the methods across various age groups in both datasets. Out of 56 tasks, our CLUDA achieves the best performance in 36 of them, where it significantly outperforms the other methods. In comparison, the best baseline methods, AdvSKM and DeepCORAL, achieve the best result in only 5 out of 56 tasks. This highlights the consistent and significant performance improvements achieved by our CLUDA in various domains.

H Ablation Study for UDA across Various Age Groups

We further conduct an ablation study to compare different variants of our CLUDA framework. Here, we build upon the previous experiments of various age groups. We use the same variants of CLUDA from the main paper (see Sec. 6.1): **w/o CL and w/o NNCL**, **w/o CL**, **w/o NNCL**, and **w/o Discriminator**. We repeat the results of **w/o UDA** and our CLUDA for better comparability. Table 15 and Table 16 list the UDA performance across age groups within MIMIC and AUMC, respectively. In addition, Tables 17 and 18 list the UDA performance across age groups from MIMIC to AUMC and from AUMC to MIMIC, respectively.

In total, our ablation study counts 56 new experiments. We report the mean over 10 random initialization. For better readability, we omitted the standard deviation. Nevertheless, we highlight performance results in bold when corresponding baselines are outperformed at a significant level.

We make the following important findings. First, our CLUDA works overall best on the target domain, thereby justifying our chosen architecture. Second, the models **w/o CL** and **w/o NNCL** perform significantly worse than our complete framework, which justifies our choice for incorporating both components. Third, we compare **w/o Discriminator** and our CLUDA. As demonstrated by our results, the discriminator is consistently responsible for better UDA for the target domain consistently. Overall, its performance improvement is significant but the gain is smaller than the other components.

Table 15: Mortality prediction between various age groups of MIMIC. Shown: mean AUROC over 10 random initializations.

Sour \mapsto Tar	w/o UDA	w/o CL and w/o NNCL	w/o CL	w/o NNCL	w/o Discriminator	CLUDA (ours)
1 \mapsto 2	0.744	0.766	0.775	0.782	0.781	0.798
1 \mapsto 3	0.685	0.715	0.740	0.735	0.735	0.747
1 \mapsto 4	0.617	0.614	0.631	0.637	0.618	0.649
2 \mapsto 1	0.818	0.820	0.838	0.836	0.842	0.856
2 \mapsto 3	0.790	0.783	0.791	0.792	0.791	0.796
2 \mapsto 4	0.696	0.674	0.688	0.705	0.676	0.697
3 \mapsto 1	0.787	0.804	0.810	0.812	0.815	0.822
3 \mapsto 2	0.833	0.845	0.838	0.844	0.840	0.843
3 \mapsto 4	0.751	0.738	0.743	0.741	0.740	0.745
4 \mapsto 1	0.783	0.779	0.791	0.782	0.784	0.807
4 \mapsto 2	0.761	0.763	0.765	0.764	0.765	0.769
4 \mapsto 3	0.736	0.742	0.744	0.738	0.743	0.748
Avg	0.750	0.754	0.763	0.764	0.761	0.773

Higher is better. Best value in bold.

Table 16: Mortality prediction between various age groups of AUMC. Shown: mean AUROC over 10 random initializations.

Sour \mapsto Tar	w/o UDA	w/o CL and w/o NNCL	w/o CL	w/o NNCL	w/o Discriminator	CLUDA (ours)
1 \mapsto 2	0.557	0.561	0.563	0.562	0.563	0.571
1 \mapsto 3	0.602	0.629	0.636	0.641	0.643	0.686
1 \mapsto 4	0.683	0.708	0.713	0.716	0.696	0.749
2 \mapsto 1	0.719	0.709	0.726	0.733	0.735	0.743
2 \mapsto 3	0.728	0.725	0.740	0.743	0.761	0.765
2 \mapsto 4	0.795	0.790	0.797	0.801	0.787	0.795
3 \mapsto 1	0.780	0.774	0.761	0.770	0.733	0.812
3 \mapsto 2	0.595	0.601	0.602	0.609	0.625	0.657
3 \mapsto 4	0.817	0.819	0.815	0.818	0.824	0.836
4 \mapsto 1	0.730	0.633	0.717	0.672	0.712	0.731
4 \mapsto 2	0.640	0.591	0.635	0.583	0.637	0.635
4 \mapsto 3	0.709	0.695	0.714	0.709	0.727	0.740
Avg	0.696	0.686	0.702	0.696	0.704	0.727

Higher is better. Best value in bold.

Table 17: Mortality prediction between various age groups from MIMIC to AUMC. Shown: mean AUROC over 10 random initializations.

Sour \mapsto Tar	w/o UDA	w/o CL and w/o NNCL	w/o CL	w/o NNCL	w/o Discriminator	CLUDA (ours)
1 \mapsto 1	0.736	0.710	0.734	0.731	0.757	0.782
1 \mapsto 2	0.628	0.686	0.717	0.703	0.714	0.731
1 \mapsto 3	0.662	0.670	0.677	0.685	0.692	0.707
1 \mapsto 4	0.754	0.734	0.747	0.735	0.758	0.754
2 \mapsto 1	0.835	0.823	0.803	0.829	0.803	0.822
2 \mapsto 2	0.629	0.615	0.637	0.638	0.668	0.705
2 \mapsto 3	0.656	0.645	0.691	0.679	0.709	0.714
2 \mapsto 4	0.773	0.772	0.785	0.796	0.794	0.807
3 \mapsto 1	0.763	0.778	0.777	0.775	0.771	0.789
3 \mapsto 2	0.627	0.684	0.685	0.676	0.665	0.691
3 \mapsto 3	0.711	0.723	0.744	0.731	0.745	0.751
3 \mapsto 4	0.782	0.789	0.788	0.804	0.797	0.796
4 \mapsto 1	0.714	0.641	0.635	0.708	0.648	0.689
4 \mapsto 2	0.668	0.578	0.685	0.590	0.660	0.673
4 \mapsto 3	0.619	0.577	0.602	0.589	0.604	0.635
4 \mapsto 4	0.758	0.707	0.753	0.735	0.760	0.768
Avg	0.707	0.696	0.716	0.713	0.722	0.738

Higher is better. Best value in bold.

Table 18: Mortality prediction between various age groups from AUMC to MIMIC. Shown: mean AUROC over 10 random initializations.

Sour \mapsto Tar	w/o UDA	w/o CL and w/o NNCL	w/o CL	w/o NNCL	w/o Discriminator	CLUDA (ours)
1 \mapsto 1	0.693	0.718	0.718	0.728	0.744	0.791
1 \mapsto 2	0.665	0.707	0.723	0.731	0.732	0.776
1 \mapsto 3	0.609	0.618	0.625	0.630	0.612	0.679
1 \mapsto 4	0.600	0.540	0.557	0.563	0.568	0.598
2 \mapsto 1	0.703	0.722	0.745	0.747	0.739	0.780
2 \mapsto 2	0.684	0.755	0.750	0.753	0.753	0.771
2 \mapsto 3	0.641	0.681	0.682	0.682	0.683	0.702
2 \mapsto 4	0.592	0.556	0.569	0.580	0.587	0.608
3 \mapsto 1	0.805	0.762	0.764	0.785	0.761	0.785
3 \mapsto 2	0.751	0.736	0.752	0.757	0.763	0.774
3 \mapsto 3	0.720	0.716	0.719	0.713	0.723	0.729
3 \mapsto 4	0.622	0.594	0.606	0.601	0.621	0.615
4 \mapsto 1	0.801	0.793	0.804	0.806	0.808	0.819
4 \mapsto 2	0.750	0.727	0.734	0.737	0.742	0.752
4 \mapsto 3	0.709	0.664	0.684	0.687	0.691	0.711
4 \mapsto 4	0.697	0.626	0.652	0.657	0.666	0.679
Avg	0.690	0.682	0.693	0.697	0.700	0.723

Higher is better. Best value in bold.

I Prediction Results of Practical Use Case

The main paper reported the average UDA performance between MIMIC and AUMC without the standard deviation of the results. Here, we provide the full results with gap filled (%) calculated for each method and additional AUPRC metric for decompensation and mortality predictions. Table 19 and Table 20 show the decompensation prediction results. Table 21 and Table 22 show the mortality prediction results. Table 23 show the length of stay prediction results.

Table 19: Decompensation prediction. Shown: AUROC (*mean* \pm *std*) over 10 random initializations.

Source	MIMIC		AUMC		Gap Filled (%)	
	Target	MIMIC	AUMC	AUMC	MIMIC	MIMIC
w/o UDA		0.831 ± 0.001	0.771 ± 0.004	0.813 ± 0.005	0.745 ± 0.004	0.0
VRADA[36]		0.817 ± 0.002	0.773 ± 0.003	0.798 ± 0.003	0.764 ± 0.002	+22.1
CoDATS[51]		0.825 ± 0.003	0.772 ± 0.004	0.818 ± 0.005	0.762 ± 0.002	+19.8
AdvSKM[29]		0.824 ± 0.002	0.775 ± 0.003	0.817 ± 0.004	0.766 ± 0.001	+24.4
CAN[25]		0.825 ± 0.002	0.773 ± 0.001	0.807 ± 0.004	0.740 ± 0.002	-5.8
CDAN[30]		0.824 ± 0.001	0.768 ± 0.003	0.817 ± 0.005	0.763 ± 0.005	+20.9
DDC[49]		0.825 ± 0.001	0.772 ± 0.004	0.819 ± 0.004	0.765 ± 0.002	+23.3
DeepCORAL[43]		0.832 ± 0.002	0.774 ± 0.003	0.819 ± 0.004	0.768 ± 0.002	+26.7
DSAN[59]		0.831 ± 0.002	0.774 ± 0.004	0.808 ± 0.004	0.759 ± 0.006	+16.3
HoMM[7]		0.829 ± 0.001	0.778 ± 0.004	0.816 ± 0.005	0.766 ± 0.001	+24.4
MMDA[38]		0.821 ± 0.001	0.766 ± 0.003	0.814 ± 0.004	0.725 ± 0.006	-23.3
CLUDA (ours)		0.832 ± 0.002	0.791 ± 0.004	0.825 ± 0.001	0.774 ± 0.002	+33.7
						+47.6

Higher is better. Best value in bold. Black font: main results for UDA. Gray font: source \leftrightarrow source.

Table 20: Decompensation prediction. Shown: AUPRC (*mean* \pm *std*) over 10 random initializations.

Source	MIMIC		AUMC		Gap Filled (%)	
	Target	MIMIC	AUMC	AUMC	MIMIC	MIMIC
w/o UDA		0.240 ± 0.003	0.208 ± 0.003	0.214 ± 0.005	0.198 ± 0.004	0.0
VRADA[36]		0.226 ± 0.003	0.209 ± 0.003	0.207 ± 0.002	0.184 ± 0.003	-33.3
CoDATS[51]		0.242 ± 0.003	0.213 ± 0.002	0.227 ± 0.002	0.211 ± 0.002	+31.0
AdvSKM[29]		0.243 ± 0.002	0.215 ± 0.001	0.230 ± 0.005	0.214 ± 0.002	+38.1
CAN[25]		0.243 ± 0.001	0.215 ± 0.002	0.213 ± 0.004	0.166 ± 0.004	-76.2
CDAN[30]		0.240 ± 0.002	0.209 ± 0.002	0.231 ± 0.002	0.217 ± 0.003	+45.2
DDC[49]		0.242 ± 0.001	0.214 ± 0.001	0.230 ± 0.001	0.211 ± 0.004	+31.0
DeepCORAL[43]		0.241 ± 0.002	0.216 ± 0.002	0.233 ± 0.002	0.213 ± 0.003	+35.7
DSAN[59]		0.249 ± 0.002	0.216 ± 0.003	0.226 ± 0.002	0.174 ± 0.002	-57.1
HoMM[7]		0.241 ± 0.002	0.215 ± 0.003	0.230 ± 0.002	0.211 ± 0.001	+31.0
MMDA[38]		0.241 ± 0.001	0.207 ± 0.004	0.227 ± 0.002	0.189 ± 0.002	-21.4
CLUDA (ours)		0.253 ± 0.003	0.223 ± 0.003	0.239 ± 0.001	0.215 ± 0.002	+40.5
						+250.0

Higher is better. Best value in bold. Black font: main results for UDA. Gray font: source \leftrightarrow source.

Table 21: Mortality prediction. Shown: AUROC (*mean* \pm *std*) over 10 random initializations.

Source	MIMIC		AUMC		Gap Filled (%)	
	Target	MIMIC	AUMC	AUMC	MIMIC	MIMIC
w/o UDA		0.831 ± 0.001	0.709 ± 0.002	0.721 ± 0.005	0.774 ± 0.006	0.0
VRADA[36]		0.827 ± 0.001	0.726 ± 0.005	0.729 ± 0.006	0.778 ± 0.002	+7.0
CoDATS[51]		0.832 ± 0.001	0.708 ± 0.005	0.724 ± 0.004	0.778 ± 0.004	+7.0
AdvSKM[29]		0.830 ± 0.001	0.707 ± 0.001	0.724 ± 0.005	0.772 ± 0.004	-3.5
CAN[25]		0.830 ± 0.001	0.719 ± 0.002	0.715 ± 0.005	0.757 ± 0.004	-29.8
CDAN[30]		0.776 ± 0.001	0.716 ± 0.006	0.712 ± 0.004	0.772 ± 0.003	-3.5
DDC[49]		0.831 ± 0.001	0.715 ± 0.005	0.721 ± 0.005	0.776 ± 0.003	+58.3
DeepCORAL[43]		0.832 ± 0.001	0.715 ± 0.005	0.727 ± 0.004	0.777 ± 0.003	+5.3
DSAN[59]		0.832 ± 0.001	0.719 ± 0.006	0.721 ± 0.006	0.747 ± 0.007	-47.4
HoMM[7]		0.833 ± 0.001	0.707 ± 0.006	0.720 ± 0.005	0.778 ± 0.002	+7.0
MMDA[38]		0.831 ± 0.001	0.718 ± 0.004	0.724 ± 0.006	0.773 ± 0.003	-1.8
CLUDA (ours)		0.836 ± 0.001	0.739 ± 0.004	0.750 ± 0.001	0.789 ± 0.002	+26.3
						+250.0

Higher is better. Best value in bold. Black font: main results for UDA. Gray font: source \leftrightarrow source.

The results confirm our findings from the main paper: overall, our CLUDA achieves the best performance in both source and target domains.

Table 22: Mortality prediction. Shown: AUPRC (*mean \pm std*) over 10 random initializations.

Source	MIMIC		AUMC		Gap Filled (%)	
	Target	MIMIC	AUMC	AUMC	MIMIC	MIMIC
w/o UDA		0.513 ± 0.004	0.412 ± 0.003	0.430 ± 0.002	0.427 ± 0.006	0.0
VRADA[36]		0.501 ± 0.003	0.419 ± 0.003	0.422 ± 0.005	0.423 ± 0.006	-4.7
CoDATS[51]		0.518 ± 0.004	0.415 ± 0.002	0.435 ± 0.004	0.441 ± 0.004	+16.3
AdvSKM[29]		0.518 ± 0.001	0.421 ± 0.001	0.441 ± 0.004	0.443 ± 0.004	+18.6
CAN[25]		0.830 ± 0.001	0.421 ± 0.002	0.436 ± 0.003	0.394 ± 0.006	-38.4
CDAN[30]		0.513 ± 0.001	0.422 ± 0.002	0.430 ± 0.001	0.435 ± 0.004	+9.3
DDC[49]		0.520 ± 0.001	0.423 ± 0.003	0.432 ± 0.004	0.442 ± 0.004	+17.4
DeepCORAL[43]		0.520 ± 0.003	0.419 ± 0.002	0.432 ± 0.003	0.435 ± 0.005	+9.3
DSAN[59]		0.514 ± 0.002	0.418 ± 0.005	0.435 ± 0.004	0.416 ± 0.007	-12.8
HoMM[7]		0.520 ± 0.002	0.418 ± 0.004	0.436 ± 0.004	0.448 ± 0.005	+24.4
MMDA[38]		0.519 ± 0.002	0.419 ± 0.004	0.441 ± 0.003	0.440 ± 0.004	+15.1
CLUDA (ours)		0.522 ± 0.002	0.428 ± 0.002	0.446 ± 0.003	0.452 ± 0.003	+29.1
						+88.9

Higher is better. Best value in bold. Black font: main results for UDA. Gray font: source \mapsto source.

Table 23: Length of stay prediction. Shown: KAPPA (*mean \pm std*) over 10 random initializations.

Source	MIMIC		AUMC		Gap Filled (%)	
	Target	MIMIC	AUMC	AUMC	MIMIC	MIMIC
w/o UDA		0.178 ± 0.002	0.169 ± 0.003	0.246 ± 0.001	0.122 ± 0.001	0.0
VRADA[36]		0.168 ± 0.003	0.161 ± 0.007	0.241 ± 0.002	0.126 ± 0.004	+7.1
CoDATS[51]		0.174 ± 0.002	0.159 ± 0.002	0.243 ± 0.001	0.120 ± 0.003	-3.6
AdvSKM[29]		0.179 ± 0.002	0.172 ± 0.005	0.244 ± 0.002	0.123 ± 0.004	+1.8
CAN[25]		0.142 ± 0.003	0.173 ± 0.004	0.233 ± 0.001	0.118 ± 0.002	-7.1
CDAN[30]		0.176 ± 0.002	0.138 ± 0.004	0.244 ± 0.002	0.124 ± 0.002	+3.6
DDC[49]		0.175 ± 0.001	0.163 ± 0.004	0.244 ± 0.001	0.123 ± 0.003	+1.8
DeepCORAL[43]		0.175 ± 0.002	0.166 ± 0.002	0.244 ± 0.001	0.126 ± 0.003	+7.1
DSAN[59]		0.175 ± 0.002	0.154 ± 0.002	0.246 ± 0.001	0.122 ± 0.003	0.0
HoMM[7]		0.174 ± 0.002	0.162 ± 0.006	0.243 ± 0.001	0.124 ± 0.001	+3.6
MMDA[38]		0.158 ± 0.002	0.093 ± 0.004	0.246 ± 0.002	0.096 ± 0.004	-46.4
CLUDA (ours)		0.216 ± 0.001	0.202 ± 0.006	0.276 ± 0.002	0.129 ± 0.003	+12.5
						+42.9

Higher is better. Best value in bold. Black font: main results for UDA. Gray font: source \mapsto source.

J Ablation Study (Additional Results)

Here, we additionally provide our ablation study for the case study presented in Sec. 6.3. Specifically, Table 24 (source: MIMIC) and Table 25 (source: AUMC) evaluate the decompensation prediction. Table 26 (source: MIMIC) and Table 27 (source: AUMC) evaluate the mortality prediction. Table 28 (source: MIMIC) and Table 29 (source: AUMC) evaluate the length of stay prediction.

Table 24: Ablation study for decompensation prediction. Shown: AUROC (*mean* \pm *std*) over 10 random initializations.

Source	MIMIC	
	MIMIC	AUMC
Target		
w/o UDA	0.831 ± 0.001	0.771 ± 0.004
w/o CL and w/o NNCL ($\lambda_{CL} = 0, \lambda_{NNCL} = 0$)	0.825 ± 0.003	0.772 ± 0.004
w/o CL ($\lambda_{CL} = 0$)	0.833 ± 0.002	0.782 ± 0.003
w/o NNCL ($\lambda_{NNCL} = 0$)	0.833 ± 0.001	0.786 ± 0.003
w/o Discriminator ($\lambda_{disc} = 0$)	0.841 ± 0.001	0.787 ± 0.003
CLUDA (ours)	0.832 ± 0.002	0.791 ± 0.004

Higher is better. Best value in bold. Black font: main results for UDA. Gray font: source \mapsto source.

Table 25: Ablation study for decompensation prediction. Shown: AUROC (*mean* \pm *std*) over 10 random initializations.

Source	AUMC	
	AUMC	MIIV
Target		
w/o UDA	0.813 ± 0.005	0.745 ± 0.004
w/o CL and w/o NNCL ($\lambda_{CL} = 0, \lambda_{NNCL} = 0$)	0.818 ± 0.005	0.761 ± 0.003
w/o CL ($\lambda_{CL} = 0$)	0.822 ± 0.004	0.763 ± 0.003
w/o NNCL ($\lambda_{NNCL} = 0$)	0.827 ± 0.001	0.771 ± 0.004
w/o Discriminator ($\lambda_{disc} = 0$)	0.832 ± 0.002	0.771 ± 0.002
CLUDA (ours)	0.825 ± 0.001	0.774 ± 0.002

Higher is better. Best value in bold. Black font: main results for UDA. Gray font: source \mapsto source.

Table 26: Ablation study for mortality prediction. Shown: AUROC (*mean* \pm *std*) over 10 random initializations.

Source	MIMIC	
	MIMIC	AUMC
Target		
w/o UDA	0.831 ± 0.001	0.709 ± 0.002
w/o CL and w/o NNCL ($\lambda_{CL} = 0, \lambda_{NNCL} = 0$)	0.830 ± 0.002	0.709 ± 0.004
w/o CL ($\lambda_{CL} = 0$)	0.836 ± 0.001	0.730 ± 0.003
w/o NNCL ($\lambda_{NNCL} = 0$)	0.840 ± 0.002	0.721 ± 0.004
w/o Discriminator ($\lambda_{disc} = 0$)	0.842 ± 0.002	0.747 ± 0.004
CLUDA (ours)	0.836 ± 0.001	0.739 ± 0.004

Higher is better. Best value in bold. Black font: main results for UDA. Gray font: source \mapsto source.

Overall, the ablation study with different variants of our CLUDA confirms the importance of each component in our framework. Specifically, our CLUDA improves the prediction performance over all of its variants in all tasks except one (mortality prediction from MIMIC to AUMC). For this task, it is important to note that the best performing variant is w/o Discriminator, which has all the novel components of our CLUDA framework.

Table 27: Ablation study for mortality prediction. Shown: AUROC (*mean* \pm *std*) over 10 random initializations.

Source	AUMC	
Target	AUMC	MIMIC
w/o UDA	0.721 ± 0.005	0.774 ± 0.006
w/o CL and w/o NNCL ($\lambda_{CL} = 0, \lambda_{NNCL} = 0$)	0.724 ± 0.004	0.778 ± 0.004
w/o CL ($\lambda_{CL} = 0$)	0.743 ± 0.001	0.781 ± 0.003
w/o NNCL ($\lambda_{NNCL} = 0$)	0.746 ± 0.004	0.781 ± 0.003
w/o Discriminator ($\lambda_{disc} = 0$)	0.749 ± 0.002	0.784 ± 0.004
CLUDA (ours)	0.750 ± 0.001	0.789 ± 0.002

Higher is better. Best value in bold. Black font: main results for UDA. Gray font: source \mapsto source.

Table 28: Ablation study for length of stay prediction. Shown: KAPPA (*mean* \pm *std*) over 10 random initializations.

Source	MIMIC	
Target	MIMIC	AUMC
w/o UDA	0.178 ± 0.002	0.169 ± 0.003
w/o CL and w/o NNCL ($\lambda_{CL} = 0, \lambda_{NNCL} = 0$)	0.173 ± 0.002	0.160 ± 0.005
w/o CL ($\lambda_{CL} = 0$)	0.212 ± 0.001	0.194 ± 0.009
w/o NNCL ($\lambda_{NNCL} = 0$)	0.212 ± 0.002	0.155 ± 0.003
w/o Discriminator ($\lambda_{disc} = 0$)	0.214 ± 0.001	0.196 ± 0.002
CLUDA (ours)	0.216 ± 0.001	0.202 ± 0.006

Higher is better. Best value in bold. Black font: main results for UDA. Gray font: source \mapsto source.

Table 29: Ablation study for length of stay prediction. Shown: KAPPA (*mean* \pm *std*) over 10 random initializations.

Source	AUMC	
Target	AUMC	MIMIC
w/o UDA	0.246 ± 0.001	0.122 ± 0.001
w/o CL and w/o NNCL ($\lambda_{CL} = 0, \lambda_{NNCL} = 0$)	0.242 ± 0.002	0.120 ± 0.003
w/o CL ($\lambda_{CL} = 0$)	0.271 ± 0.002	0.122 ± 0.003
w/o NNCL ($\lambda_{NNCL} = 0$)	0.274 ± 0.001	0.113 ± 0.001
w/o Discriminator ($\lambda_{disc} = 0$)	0.274 ± 0.001	0.125 ± 0.004
CLUDA (ours)	0.276 ± 0.002	0.129 ± 0.003

Higher is better. Best value in bold. Black font: main results for UDA. Gray font: source \mapsto source.

K CLUDA with SimCLR

In our CLUDA framework, we capture contextual representation in time series data by leveraging contrastive learning. Specifically, we adapt momentum contrast (MoCo) [21] for contrastive learning in our framework. This choice is motivated by earlier research from other domains [21, 9, 55, 12], where MoCo was found to yield more stable negative samples (due to the momentum-updated feature extractor) as compared to other approaches throughout each training step, such as SimCLR[8]. In principle, stability yields stronger negative samples for the contrastive learning objectives and, therefore, increases the mutual information between the positive pair (i. e., two augmented views of the same sample). Furthermore, MoCo allows storing the negative samples within a queue, facilitating a larger number of negative samples for the contrastive loss as compared to SimCLR. As shown earlier [2, 46, 47], the lower bound of the mutual information between the positive pair increases with a larger number of negative samples in CL. With that motivation, we opted for MoCo [21] in our CLUDA instead of SimCLR[8]. Nevertheless, we evaluate our choice through numerical experiments below.

We now further perform an ablation study where we repeat the experiments with SimCLR (instead of MoCo) for our case study from Sec. 6.3. Specifically, we provide results for decompensation prediction (see Table 30), mortality prediction (see Table 31), and length of stay prediction (see Table 32).

Table 30: Decompensation prediction. Shown: AUROC (*mean* \pm *std*) over 10 random initializations.

Source	MIMIC		AUMC	
	Target	MIMIC	AUMC	AUMC
w/o UDA	0.831 \pm 0.001	0.771 \pm 0.004	0.813 \pm 0.005	0.745 \pm 0.004
CLUDA w/ SimCLR	0.826 \pm 0.001	0.776 \pm 0.001	0.801 \pm 0.005	0.751 \pm 0.005
CLUDA (ours)	0.832 \pm 0.002	0.791 \pm 0.004	0.825 \pm 0.001	0.774 \pm 0.002

Higher is better. Best value in bold. Black font: main results for UDA. Gray font: source \mapsto source.

Table 31: Mortality prediction. Shown: AUROC (*mean* \pm *std*) over 10 random initializations.

Source	MIMIC		AUMC	
	Target	MIMIC	AUMC	AUMC
w/o UDA	0.831 \pm 0.001	0.709 \pm 0.002	0.721 \pm 0.005	0.774 \pm 0.006
CLUDA w/ SimCLR	0.827 \pm 0.001	0.724 \pm 0.004	0.748 \pm 0.002	0.781 \pm 0.002
CLUDA (ours)	0.836 \pm 0.001	0.739 \pm 0.004	0.750 \pm 0.001	0.789 \pm 0.002

Higher is better. Best value in bold. Black font: main results for UDA. Gray font: source \mapsto source.

Table 32: Length of stay prediction. Shown: KAPPA (*mean* \pm *std*) over 10 random initializations.

Source	MIMIC		AUMC	
	Target	MIMIC	AUMC	AUMC
w/o UDA	0.178 \pm 0.002	0.169 \pm 0.003	0.246 \pm 0.001	0.122 \pm 0.001
CLUDA w/ SimCLR	0.203 \pm 0.001	0.178 \pm 0.006	0.258 \pm 0.005	0.107 \pm 0.003
CLUDA (ours)	0.216 \pm 0.001	0.202 \pm 0.006	0.276 \pm 0.002	0.129 \pm 0.003

Higher is better. Best value in bold. Black font: main results for UDA. Gray font: source \mapsto source.

The results confirm our choice for MoCo instead of SimCLR in capturing the contextual representation in time series. Specifically, our CLUDA improves the result of CLUDA w/ SimCLR in all tasks by a large margin. Despite being inferior to our CLUDA, CLUDA w/ SimCLR achieves better UDA performance compared to other baseline methods in decompensation prediction from MIMIC to

AUMC, mortality prediction from AUMC to MIMIC, and length of stay prediction from MIMIC to AUMC. This shows the importance of leveraging the contextual representation into unsupervised domain adaptation. Besides, it highlights that our CLUDA can be further improved in the future with the recent advances in capturing the contextual representation of time series.